

CERN-EP-2018-319

28 November 2018

Study of J/ψ azimuthal anisotropy at forward rapidity in Pb–Pb collisions at $\sqrt{s_{NN}} = 5.02$ TeV

ALICE Collaboration*

Abstract

The second (v_2) and third (v_3) flow harmonic coefficients of J/ψ mesons are measured at forward rapidity ($2.5 < y < 4.0$) in Pb–Pb collisions at $\sqrt{s_{NN}} = 5.02$ TeV with the ALICE detector at the LHC. Results are obtained with the scalar product method and reported as a function of transverse momentum, p_T , for various collision centralities. A positive value of J/ψ v_3 is observed with 3.7σ significance. The measurements, compared to those of prompt D^0 mesons and charged particles at mid-rapidity, indicate an ordering with $v_n(J/\psi) < v_n(D^0) < v_n(h^\pm)$ ($n = 2, 3$) at low and intermediate p_T up to 6 GeV/ c and a convergence with $v_2(J/\psi) \approx v_2(D^0) \approx v_2(h^\pm)$ at high p_T above 6–8 GeV/ c . In semi-central collisions (5–40% and 10–50% centrality intervals) at intermediate p_T between 2 and 6 GeV/ c , the ratio v_3/v_2 of J/ψ mesons is found to be significantly lower (4.6σ) with respect to that of charged particles. In addition, the comparison to the prompt D^0 -meson ratio in the same p_T interval suggests an ordering similar to that of the v_2 and v_3 coefficients. The J/ψ v_2 coefficient is further studied using the Event Shape Engineering technique. The obtained results are found to be compatible with the expected variations of the eccentricity of the initial-state geometry.

1 Introduction

The study of collisions of ultra-relativistic heavy ions aims to characterize the Quark–Gluon Plasma (QGP), a strongly coupled state of matter comprising of deconfined quarks and gluons. One of the main features of heavy-ion collisions is the anisotropic particle flow [1, 2]. It arises from initial collision geometry anisotropies being converted by the pressure gradients of the QGP medium to final-state particle momentum anisotropies. The anisotropic flow is described by the coefficients v_n of a Fourier series decomposition of the azimuthal distribution of the produced particles [3]

$$\frac{dN}{d\varphi} \propto 1 + 2 \sum_{n=1}^{\infty} v_n \cos[n(\varphi - \Psi_n)], \quad (1)$$

where φ is the azimuthal angle of the particle and Ψ_n is the n -th harmonic symmetry plane angle. The dominant second-order flow coefficient (v_2) is called elliptic flow and mostly originates from the almond-shaped overlap area between the colliding nuclei in non-central collisions. The third-order flow coefficient (v_3) is named triangular flow and is generated by fluctuations in the initial distribution of nucleons in the overlap region [4–8].

Heavy quarks, in particular their bound quark-antiquark states known as quarkonia, are important probes of the QGP. Heavy-quark pairs are created prior to the formation of the QGP through hard parton collisions and thus experience the full evolution of the system. Measurements of the J/ψ nuclear modification factor (R_{AA}) as a function of centrality in Pb–Pb collisions at the LHC [9–11] are reproduced by transport [12–14] and statistical hadronization [15, 16] models including partial to full J/ψ (re)generation by recombination of thermalized charm quarks. Such (re)generation component is dominant at low transverse momentum (p_T) as shown by the comparison [11, 17] of the R_{AA} as function of p_T with transport model calculations. In the case of the statistical hadronization model, the produced J/ψ reflects the dynamics of the charm quarks at the QGP phase boundary. The measured p_T spectra seem to support this idea [18]. Measurements of the azimuthal anisotropies of J/ψ production in high-energy heavy-ion collisions can bring new important insights on the charm quark dynamics.

A recent measurement of the elliptic flow of J/ψ at forward rapidity in central and semi-central Pb–Pb collisions at the center of mass energy per nucleon pair of $\sqrt{s_{NN}} = 5.02$ TeV indicates a significant positive v_2 coefficient [19]. This result is compatible with the hypothesis of J/ψ production via recombination of thermalized c and \bar{c} quarks from the QGP medium predominantly at low p_T , but the magnitude and the transverse momentum dependence of the v_2 coefficient differ significantly from theoretical calculations [12–14]. Moreover, the v_2 coefficient is found to be quite significant at high p_T , in contrast with the expectations of small azimuthal asymmetry originating mainly from path-length dependent J/ψ dissociation in the medium. Furthermore, a positive J/ψ v_2 coefficient at intermediate and high p_T has been observed in p–Pb collisions [20, 21], in which neither a significant contribution from charm-quark recombination nor sizable path-length effects are expected [22]. Recent measurements of D-meson azimuthal asymmetry in Pb–Pb collisions are interpreted as collective behavior of the charm quarks at low p_T and path-length dependent charm-quark energy loss at high p_T [23, 24].

Hydrodynamic calculations [25] show that $v_n \approx \kappa_n \epsilon_n$ for $n = 2$ and 3, where ϵ_n is the eccentricity coefficient of the initial-state collision geometry. The parameters κ_n encode the response of the QGP medium and depend on the particle type and mass as well as its transverse momentum. At low p_T , the flow coefficients of light-flavoured particles increase with increasing p_T [26, 27]. This increase of v_n coefficients as a function of p_T depends of the particle mass and can be attributed to the radial expansion of the QGP medium. At 3–4 GeV/ c , the flow coefficients reach a maximum. The position of the maximum, divided by the number of constituent quarks n_q , does not depend strongly on the particle mass as predicted by coalescence models [28]. Furthermore, the v_n values at the maximum, divided by n_q , are similar for all measured light-flavoured particles, with deviations of up to $\pm 20\%$ between mesons and baryons [27]. At high p_T above 6–8 GeV/ c , the observed azimuthal anisotropy of the final-state particles is believed

to come from path-length dependent parton energy loss inside the QGP. Calculations [29] show that the corresponding v_2 and v_3 coefficients exhibit approximately linear dependence on ε_2 and ε_3 , respectively. Nevertheless, the correlation between the flow coefficients and the initial-state eccentricities is weaker with respect to the hydrodynamic case, especially between v_3 and ε_3 . Interestingly, the particle-mass dependence of v_2 and v_3 appears to be strongly reduced in the ratio v_3/v_2 in semi-central collisions for light-flavored particles [27]. Whether the above considerations also hold for heavy quarks and quarkonia is an open question whose answer could help to understand the origin of charm quark azimuthal anisotropies and characterize their interactions with the flowing medium.

In the present analysis, the J/ψ v_2 and v_3 coefficients as well as the ratio v_3/v_2 as a function of the transverse momentum and the collision centrality are measured. Wherever possible, the data are compared to existing mid-rapidity charged-particle (predominantly π^\pm) and prompt D^0 -meson results. In addition, the dependence of the J/ψ v_2 coefficient on the initial-state conditions is studied with the Event Shape Engineering (ESE) technique [30]. Fluctuations in the initial-state energy density distribution lead to event-by-event variations of the flow observed at a given centrality [31]. The ESE technique consists of selecting events with the same centrality but different flow and therefore initial-state geometry eccentricity [32, 33]. Recently, the ESE technique has been applied to the measurement of mid-rapidity D-meson production in Pb–Pb collisions at $\sqrt{s_{NN}} = 5.02$ TeV [34]. The obtained results indicate a correlation between the D-meson azimuthal anisotropy and the flow of light-flavoured particles.

The J/ψ mesons are reconstructed at forward rapidity ($2.5 < y < 4.0$) via their $\mu^+\mu^-$ decay channel. The measured J/ψ mesons originate from both prompt J/ψ (direct and from decays of higher-mass charmonium states) and non-prompt J/ψ (feed down from b-hadron decays) production.

This letter is organized as follows. A brief description of the ALICE apparatus and the data sample used is given in Sec. 2. Section 3 outlines the employed analysis technique. The evaluation of the systematic uncertainties is discussed in Sec. 4, while the results are reported in Sec. 5. Finally, conclusions are presented in Sec. 6.

2 Experimental setup and data sample

The ALICE detectors essential for the present analysis are briefly described below. A full overview of the ALICE apparatus and its performance can be found in Refs. [35, 36]. The muon spectrometer, which covers the pseudorapidity range $-4 < \eta < -2.5$, is used to reconstruct muon tracks. The spectrometer consists of a front absorber followed by five tracking stations. The third station is placed inside a dipole magnet. The tracking stations are complemented by two trigger stations located downstream behind an iron wall. The Silicon Pixel Detector (SPD) [37] is employed to reconstruct the position of the primary vertex and to determine the flow direction. The SPD consists of two cylindrical layers covering $|\eta| < 2.0$ and $|\eta| < 1.4$, respectively. It is placed in the central barrel of ALICE. The central barrel is operated inside a solenoidal magnetic field parallel to the beam line. The SPD is also used to reconstruct the so-called tracklets, track segments formed by the clusters in the two SPD layers and the primary vertex [38]. The V0 detector [39] consists of two arrays of 32 scintillator counters each, covering $2.8 < \eta < 5.1$ (V0A) and $-3.7 < \eta < -1.7$ (V0C), respectively. It provides the minimum-bias (MB) trigger and is used for event selection and determination of collision centrality [40]. In addition, two tungsten-quartz neutron Zero Degree Calorimeters (ZDCs), installed 112.5 meters from the interaction point along the beam line on each side, are used for event selection.

The present analysis is based on the data sample of Pb–Pb collisions collected by ALICE in 2015 at $\sqrt{s_{NN}} = 5.02$ TeV. The trigger required coincidence of MB and dimuon triggers. The MB trigger was provided by the V0 detector requesting signals in both V0A and V0C arrays. The dimuon unlike-sign trigger required at least a pair of opposite-sign track segments in the muon trigger stations. The transverse momentum threshold of the trigger algorithm was set such that the efficiency for muon tracks with p_T

= 1 GeV/ c is 50%. The sample of single muons or like-sign dimuons were collected using the same trigger algorithm, but requiring at least one track segment or at least a pair of like-sign track segments, respectively. The integrated luminosity of the analyzed data sample is about $225 \mu\text{b}^{-1}$.

The beam-induced background is filtered out offline by applying a selection based on the V0 and the ZDC timing information [41]. The interaction pile-up is removed by exploiting the correlations between the number of clusters in the SPD, the number of reconstructed SPD tracklets and the total signal in the V0A and V0C detectors. The primary vertex position is required to be within ± 10 cm from the nominal interaction point along the beam direction. The data are split in intervals of collision centrality, which is obtained based on the total signal in the V0A and V0C detectors [40].

The muon selection is identical to that used in Ref. [20]. The dimuons are reconstructed in the acceptance of the muon spectrometer ($2.5 < y < 4.0$) and are required to have a transverse momentum between 0 and 12 GeV/ c .

3 Analysis

The flow coefficients v_n of the selected dimuons are measured using the scalar product (SP) method [2, 42], in which they are calculated from the expression

$$v_n\{\text{SP}\} = \frac{\langle\langle \mathbf{u}_n \mathbf{Q}_n^{\text{SPD}*} \rangle\rangle}{R_n}, \quad (2)$$

$$R_n = \sqrt{\frac{\langle\langle \mathbf{Q}_n^{\text{SPD}} \mathbf{Q}_n^{\text{V0A}*} \rangle\rangle \langle\langle \mathbf{Q}_n^{\text{SPD}} \mathbf{Q}_n^{\text{V0C}*} \rangle\rangle}{\langle\langle \mathbf{Q}_n^{\text{V0A}} \mathbf{Q}_n^{\text{V0C}*} \rangle\rangle}},$$

where $\mathbf{u}_n = \exp(in\varphi)$ is the unit flow vector of the dimuon, $\mathbf{Q}_n^{\text{SPD}}$, $\mathbf{Q}_n^{\text{V0A}}$ and $\mathbf{Q}_n^{\text{V0C}}$ are the event flow vectors measured in the SPD, V0A and V0C detectors, respectively, and n is the harmonic number. The brackets $\langle \dots \rangle$ denote an average over all events, the double brackets $\langle\langle \dots \rangle\rangle$ an average over all particles in all events, and $*$ the complex conjugate. The SPD event flow vector $\mathbf{Q}_n^{\text{SPD}}$ is calculated from the azimuthal distribution of the reconstructed SPD tracklets. The V0A and V0C event flow vectors $\mathbf{Q}_n^{\text{V0A}}$ and $\mathbf{Q}_n^{\text{V0C}}$ are calculated from the azimuthal distribution of the signal in the V0 detector. The components of all three event flow vectors are corrected for non-uniform detector acceptance and efficiency using a recentering procedure (i.e. by subtracting of the \mathbf{Q}_n -vector averaged over many events from the \mathbf{Q}_n -vector of each event) [43]. The denominator R_n in the above equation is called resolution and is obtained as a function of collision centrality. The gap in pseudorapidity between \mathbf{u}_n and $\mathbf{Q}_n^{\text{SPD}}$ ($|\Delta\eta| > 1.0$) suppresses short-range correlations (“non-flow”), which are unrelated to the azimuthal asymmetry in the initial geometry and come from jets and resonance decays [19]. In the following, the $v_n\{\text{SP}\}$ coefficients are denoted as v_n .

The J/ψ flow coefficients are extracted by a fit of the superposition of the J/ψ signal and the background to the dimuon flow coefficients as a function of the dimuon invariant mass [44]

$$v_n(M_{\mu\mu}) = \frac{N^{J/\psi}}{N^{J/\psi} + N_{+-}^{\text{B}}} v_n^{J/\psi} + \frac{N_{+-}^{\text{B}}}{N^{J/\psi} + N_{+-}^{\text{B}}} v_n^{\text{B}}(M_{\mu\mu}), \quad (3)$$

where $v_n^{J/\psi}$ is the flow coefficient of the signal and v_n^{B} is the $M_{\mu\mu}$ -dependent flow coefficient of the background. The $N^{J/\psi}$ and N_{+-}^{B} are the signal and the background dimuon yields, respectively, as a function of $M_{\mu\mu}$. They are obtained by fitting the $M_{\mu\mu}$ distribution with a mixture of an extended Crystal Ball (CB2) function for the J/ψ signal and a Variable-Width Gaussian (VWG) function for the background [45]. The J/ψ peak position and width are left free, while the CB2 tail parameters are fixed to the values reported in Ref. [46]. The statistical uncertainties of $N^{J/\psi}$ and N_{+-}^{B} are not considered in the fit of $v_n(M_{\mu\mu})$, given their negligible contribution to the statistical uncertainty of the $v_n^{J/\psi}$ coefficient. The

$\psi(2S)$ signal is not included in the fit of $v_n(M_{\mu\mu})$ because of its extremely low significance in central and semi-central collisions.

In previous measurements [19, 20], the $M_{\mu\mu}$ dependence of the background flow coefficients was parameterized by an arbitrary function. This approach leads to an increase of the statistical uncertainty of the J/ψ flow coefficients, because the parameters of the function are not fixed. Moreover, an additional systematic uncertainty arises from the fact that the functional form of the background distribution is unknown. In the present analysis, we adopt a different approach. It is known that, in collisions of heavy ions, the dimuon background in the vicinity of the J/ψ is mostly combinatorial and can be described satisfactorily with the event-mixing technique [9, 17]. This technique consists in forming dimuons by combining muons from two different events having similar collision centrality. The flow coefficients of the combinatorial background are fully determined by the flow coefficients of the single muons from which the background dimuons are formed. One can show that for any given kinematical configuration of the background dimuon, its flow coefficients can be expressed as

$$v_n^B(M_{\mu\mu}) = \frac{\langle v_n^{(1)}(p_T^{(1)}, \eta_1) \cos[n(\varphi_1 - \varphi)] + v_n^{(2)}(p_T^{(2)}, \eta_2) \cos[n(\varphi_2 - \varphi)] \rangle_{M_{\mu\mu}}}{\langle 1 + 2 \sum_{m=1}^{\infty} v_m^{(1)}(p_T^{(1)}, \eta_1) v_m^{(2)}(p_T^{(2)}, \eta_2) \cos[m(\varphi_1 - \varphi_2)] \rangle_{M_{\mu\mu}}}, \quad (4)$$

where $v_n^{(1)}(p_T^{(1)}, \eta_1)$ and $v_n^{(2)}(p_T^{(2)}, \eta_2)$ are the flow coefficients of the two muons as a function of their transverse momenta and pseudorapidities, φ_1 and φ_2 are the azimuthal angles of the two muons and φ is the azimuthal angle of the dimuon. The brackets $\langle \dots \rangle_{M_{\mu\mu}}$ denote an average over all dimuons ($p_T^{(1)}, p_T^{(2)}, \eta_1, \eta_2, \varphi_1, \varphi_2$) that belong to any given $M_{\mu\mu}$ interval. The details on the derivation of Eq.(4) are given in appendix A. In case of the event mixing, the numerator in Eq. (4) is calculated as

$$\left\langle \frac{\mathbf{u}_n^{(1)} \mathbf{Q}_n^{(1), \text{SPD}}}{R_n^{(1)}} \cos(n(\varphi_1 - \varphi)) + \frac{\mathbf{u}_n^{(2)} \mathbf{Q}_n^{(2), \text{SPD}}}{R_n^{(2)}} \cos(n(\varphi_2 - \varphi)) \right\rangle_{M_{\mu\mu}}, \quad (5)$$

where $\mathbf{u}_n^{(1)}$ and $\mathbf{u}_n^{(2)}$ are the unit vector of the two muons, $\mathbf{Q}_n^{(1)}$ and $\mathbf{Q}_n^{(2)}$ are the SPD flow vectors for the events containing the two muons, and $R_n^{(1)}$ and $R_n^{(2)}$ are their resolutions. The brackets $\langle \dots \rangle_{M_{\mu\mu}}$ denote an average over all mixed-event dimuons belonging to any given $M_{\mu\mu}$ interval. The denominator in Eq. (4) reflects the modification of the dimuon yield due to the flow of single muons. Since the event flow vectors of the two mixed events are not correlated, the mixed-event dimuon yield is not modified by the single muon flow. Thus, the denominator is obtained directly as the ratio $N_{+-}^B/N_{+-}^{\text{mix}}$, where N_{+-}^{mix} is the number of mixed-event unlike-sign dimuons as a function of $M_{\mu\mu}$. The ratio is calculated after a proper normalization of N_{+-}^{mix} using the like-sign dimuons from the same and mixed events. The normalization factor is obtained as [17]

$$\frac{\int_{M_{\mu\mu}} N_{+-}^{\text{mix}} \sqrt{\frac{N_{++}^{\text{same}} N_{--}^{\text{same}}}{N_{++}^{\text{mix}} N_{--}^{\text{mix}}}} dM_{\mu\mu}}{\int_{M_{\mu\mu}} N_{+-}^{\text{mix}} dM_{\mu\mu}}, \quad (6)$$

where $N_{++}^{\text{same}}(N_{--}^{\text{same}})$ and $N_{++}^{\text{mix}}(N_{--}^{\text{mix}})$ are the numbers of like-sign (positive and negative charges) same-event and mixed-event dimuons, respectively. The integral is calculated in the invariant mass interval between 2.2 and 4.5 GeV/c². Assuming a purely combinatorial background, the $v_n^B(M_{\mu\mu})$ coefficient, obtained with the event-mixing procedure described above, is used directly in order to fix the background term of the fit from Eq. (3). All the analysis steps discussed in this section are performed separately in each considered dimuon transverse momentum and centrality interval. The event mixing and the normalization of N_{+-}^{mix} are done in 5%-wide collision centrality intervals.

Examples of the $M_{\mu\mu}$ fit and the mixed-event distribution N_{+-}^{mix} as a function of $M_{\mu\mu}$ in several centrality and p_T intervals are shown in Fig. 1. At low and intermediate p_T , the mixed-event distribution describes

the dimuon background on a percent level with a residual difference presumably originating from the single muon flow. However, at high p_T , this difference becomes much larger (up to $\approx 35\%$ in the vicinity of the J/ψ mass in $8 < p_T < 12$ GeV/ c and 30–50% centrality interval) and goes beyond a possible single muon flow contribution. This points to the presence of a correlated dimuon background. Such a background is believed to originate from production of heavy-flavor quark pairs and to become significant in semi-central and peripheral collisions at high p_T [47, 48].

Examples of the $v_2(M_{\mu\mu})$ fit based on the analysis approach described above are presented in Fig. 2. As can be seen, the fit performs quite satisfactorily, with the mixed-event v_2 coefficient being able to describe the shape and amplitude of the background v_2 in the entire considered invariant mass interval from 1.5 to 4.5 GeV/ c^2 . This is not surprising at low and intermediate p_T , where the mixed-event dimuon distribution describes rather precisely the background dimuon distribution (top and middle panels in Figs. 1 and 2). Remarkably, however, the mixed-event approach performs satisfactorily also at high p_T in semi-central collisions, where the contribution of the correlated background is significant (bottom right panels in Figs. 1 and 2). Given that the denominator in Eq. (4) is obtained as the ratio $N_{+-}^B/N_{+-}^{\text{mix}}$, this means that the flow coefficient of the correlated background is significantly lower than that of the combinatorial one. The systematic effect arising from the presence of the correlated background and the corresponding uncertainties are discussed in Section 4. The approach described above performs equally well also in case of the v_3 coefficient. This is illustrated in Fig. 3, where the fits of the centrality and p_T -integrated $v_2(M_{\mu\mu})$ and $v_3(M_{\mu\mu})$ distributions are compared.

The Event Shape Engineering (ESE) technique is performed following the procedure described in Ref. [33]. It is based on the magnitude of the second-order reduced V0A event flow vector defined as in Ref. [42]

$$q_2^{\text{V0A}} = \frac{|\mathbf{Q}_2^{\text{V0A}}|}{\sqrt{S^{\text{V0A}}}}, \quad (7)$$

where $|\mathbf{Q}_2^{\text{V0A}}|$ is the magnitude of the second-order V0A event flow vector and S^{V0A} is the total signal in the V0A detector. The large pseudorapidity gap between the V0A and the muon spectrometer ($|\Delta\eta| > 5.3$) greatly suppresses the non-flow contribution and guarantees a proper event-shape selection. Two event-shape classes with the lowest and highest q_2^{V0A} values corresponding to the 0–20% and 80–100% intervals, respectively, are investigated for the 5–40% centrality interval.

4 Systematic uncertainties

The systematic effect related to the presence of correlated background is checked by modifying the definition of the background coefficient $v_2^B(M_{\mu\mu})$. The ratio $N_{+-}^B/N_{+-}^{\text{mix}}$ is replaced by $N_{+-}^B/(N_{+-}^{\text{mix}} + \alpha(N_{+-}^B - N_{+-}^{\text{mix}}))$, where the parameter α represents the strength of the flow of the correlated background. The value of 0 corresponds to the default approach (e.g. assuming negligible flow of the correlated background), while the value of 1 corresponds to the assumption that the correlated background has the same flow coefficient as compared to the combinatorial background. The parameter α is left free in the fit of Eq. (3) and the differences in the resulting J/ψ v_2 with respect to the default approach are taken as systematic uncertainties. As expected, in central (0–10%) collisions and at low transverse momentum, the uncertainties are practically negligible. In semi-central (30–50% centrality interval) collisions and in the highest considered transverse momentum interval ($8 < p_T < 12$ GeV/ c), the uncertainty of the J/ψ v_2 reaches 0.013. The parameter α is found to be well below 1 in all centrality and p_T intervals. The corresponding systematic uncertainty of the J/ψ v_3 coefficient is in general significantly smaller. No clear pattern is found as a function of collision centrality and p_T . Conservatively, the parameter α is fixed to 1 and the difference in the results with respect to the ones obtained with default value of 0 is taken as systematic uncertainty. It is worth noting that even though the fraction of correlated background at high p_T in semi-central collisions is significant, its effect on the J/ψ flow coefficients is suppressed by the high signal-to-background ratio $N^{J/\psi}/N_{+-}^B$. As described in appendix A, a small additional $v_2^{(1)}v_4^{(2)} + v_2^{(2)}v_4^{(1)}$

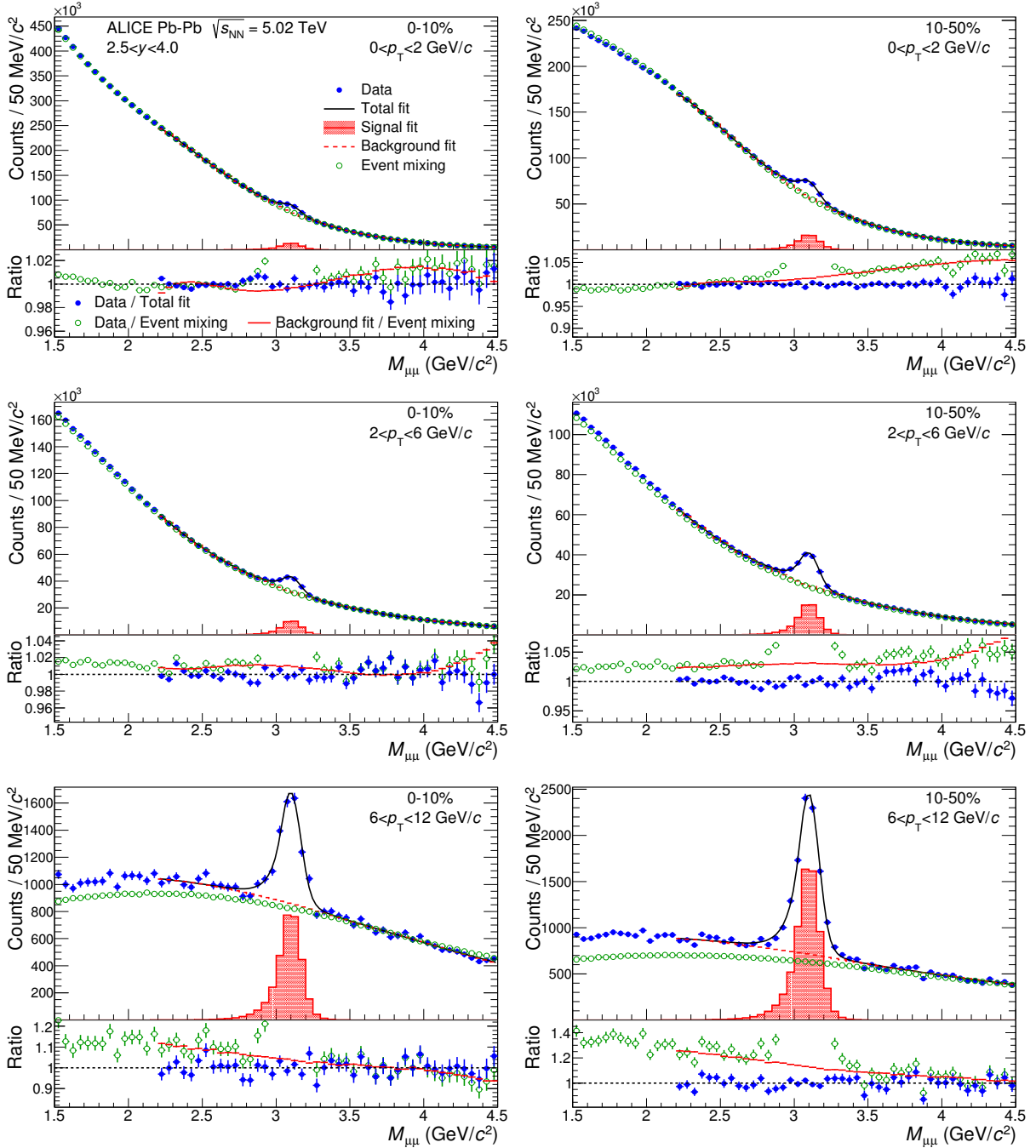


Fig. 1: (Color online) The $M_{\mu\mu}$ distribution in low (top panels), intermediate (middle panels) and high (bottom panels) p_T intervals for central (left panels) and semi-central (right panels) collisions. The data are fitted to a combination of an extended Crystal Ball (CB2) function for the signal and a Variable-Width Gaussian (VWG) function for the background. The distributions are compared to the ones obtained with the event-mixing technique (see text for details). Only statistical uncertainties are shown.

term is present in v_2^B . Its estimated contribution is added to the fit to the $v_2(M_{\mu\mu})$ distribution and the change in the J/ψ v_2 results with respect to the default approach is taken as systematic uncertainty. These uncertainties are found to be sizable only in $0 < p_T < 2$ GeV/c and 10–50% centrality interval, where they reach 0.002.

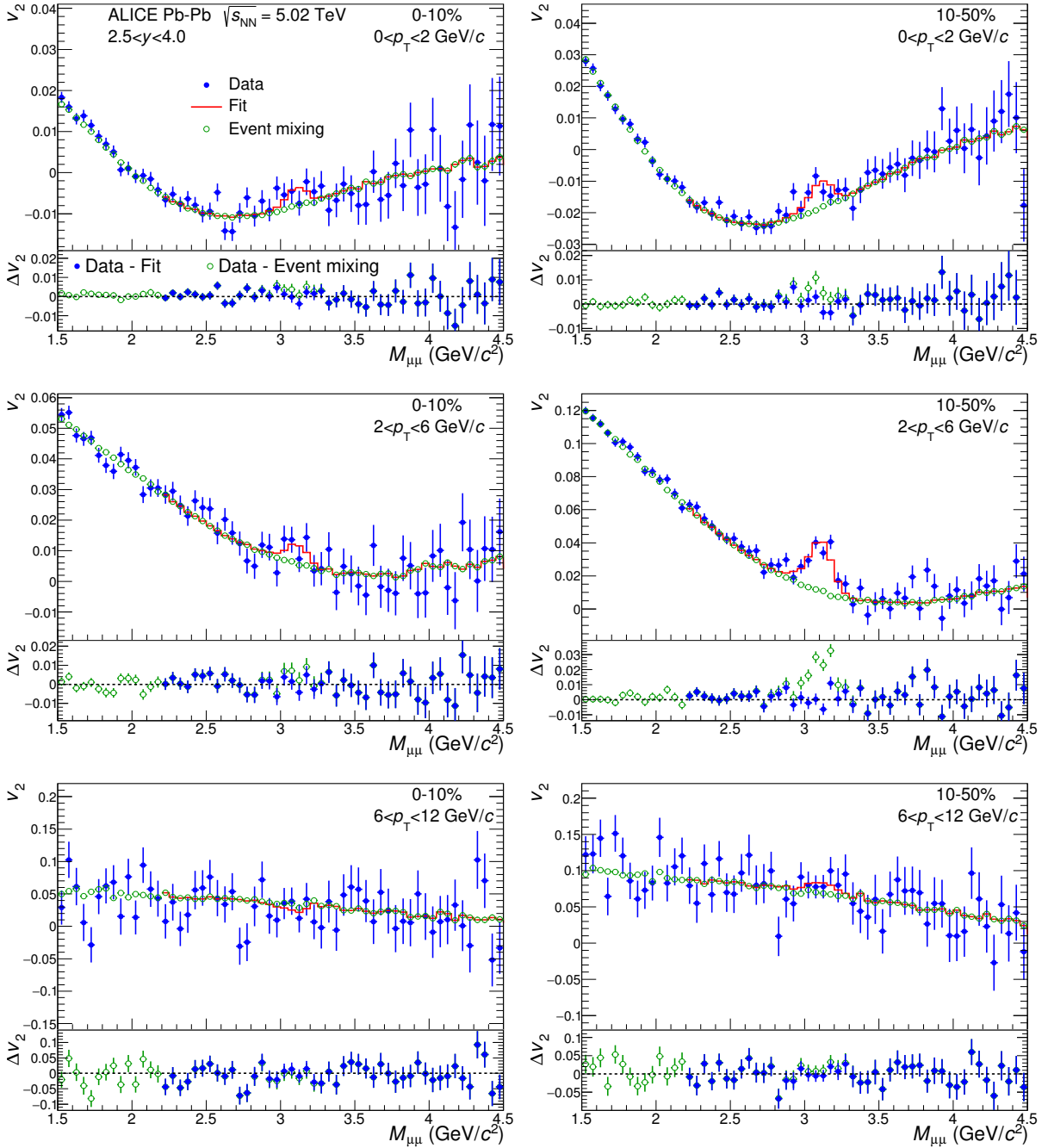


Fig. 2: (Color online) The $v_2(M_{\mu\mu})$ distribution in low (top panels), intermediate (middle panels) and high (bottom panels) p_T intervals for central (left panels) and semi-central (right panels) collisions. The data are fitted with the function from Eq. 3, where the background coefficient $v_2^B(M_{\mu\mu})$ is fixed using the event-mixing procedure. The background coefficient $v_2^B(M_{\mu\mu})$ alone down to 1.5 GeV/c² is also presented. Only statistical uncertainties are shown.

The systematic uncertainty related to the signal-to-background ratio $N^{J/\psi}/N_{+-}^B$ in Eq. (3) is estimated by varying the signal tails (e.g. the parameters describing the tails of the CB2 function, employed to fit the signal peak), the background fit functions and the fit range [19, 20]. The obtained uncertainties are up to 0.001.

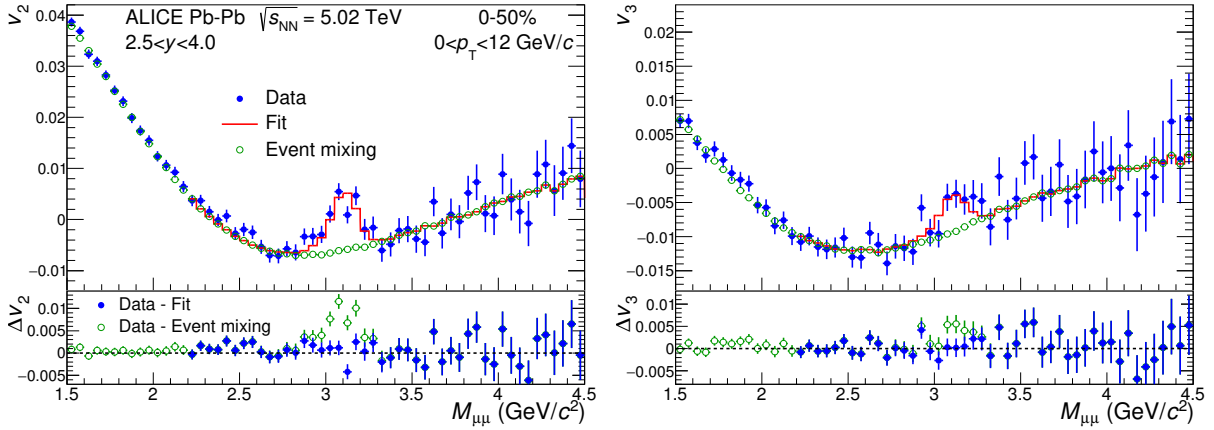


Fig. 3: (Color online) The $v_2(M_{\mu\mu})$ (left panel) and $v_3(M_{\mu\mu})$ (right panel) distributions in the 0–50% centrality and $0 < p_T < 12$ GeV/c. The distributions are fitted with the function from Eq. 3, where the background coefficients $v_2^B(M_{\mu\mu})$ and $v_3^B(M_{\mu\mu})$ are fixed using the event-mixing procedure. The background coefficients alone down to 1.5 GeV/c² are also presented. Only statistical uncertainties are shown.

The effect of any residual non-uniform detector acceptance and efficiency in the calculation of the SPD event flow vector is checked via the imaginary part of the scalar product defined in Eq. (2) [49]. No systematic uncertainty is assigned as the terms are consistent with zero within statistical uncertainties. The resolution of the SPD event flow vector is calculated from the events containing at least one selected dimuon by default. Alternatively, it is calculated from all events recorded with the MB trigger and passing the offline event selection, as well as from the events containing at least one selected single muon. Differences up to 1% and 2% with respect to the default approach are observed for R_2 and R_3 , respectively, and are taken as systematic uncertainties. For the event-shape classes, a bias can arise from auto-correlations due to the usage of the VOA event flow vector for both q_2 and R_2 . This potential bias is assessed by replacing the ratio $\langle \mathbf{Q}_n^{\text{SPD}} \mathbf{Q}_n^{\text{VOA}*} \rangle / \langle \mathbf{Q}_n^{\text{VOA}} \mathbf{Q}_n^{\text{VOC}*} \rangle$ in Eq. 2 with the one from the unbiased data sample. The resulting effect is smaller than 1% and is neglected.

The muon spectrometer occupancy affects the reconstruction efficiency and thus can bias (lower) the measured v_n coefficients. The reconstruction efficiency as a function of centrality is taken from Ref. [11], where it is obtained by embedding simulated $J/\psi \rightarrow \mu^+ \mu^-$ decays into real Pb–Pb events. It is found to decrease linearly with the signal in the V0C detector S^{V0C} , which largely covers the geometrical acceptance of the muon spectrometer. Thus, the systematic deviations of the J/ψ v_n are calculated as the product of the single muon v_n , the first derivative of the reconstruction efficiency with respect to S^{V0C} and the mean $\langle S^{\text{V0C}} \rangle$ in the considered centrality interval. The single muon v_n coefficients are obtained with the same SP approach as the one employed for J/ψ . Conservatively, the maximum of the single muon v_n as a function of p_T is used. The typical values of these systematic deviations are found to be up to 0.0025 and 0.0015 for the J/ψ v_2 and v_3 , respectively. Given the small magnitude of the effect, we do not correct the measured coefficients, but take the above deviations as systematic uncertainties.

5 Results

Figure 4 shows the measured J/ψ v_2 and v_3 coefficients as a function of the transverse momentum for three centrality intervals. The results are compared to the v_2 and v_3 coefficients of charged particles [50] and prompt D^0 mesons [23] at mid-rapidity obtained with the SP method and a pseudo-rapidity gap $|\Delta\eta| > 2.0$ between the particle of interest and the kinematic interval of the event flow vector calculation. At low and intermediate p_T , up to 6 GeV/c, one can observe a clear ordering with $v_n(J/\psi) < v_n(D^0) <$

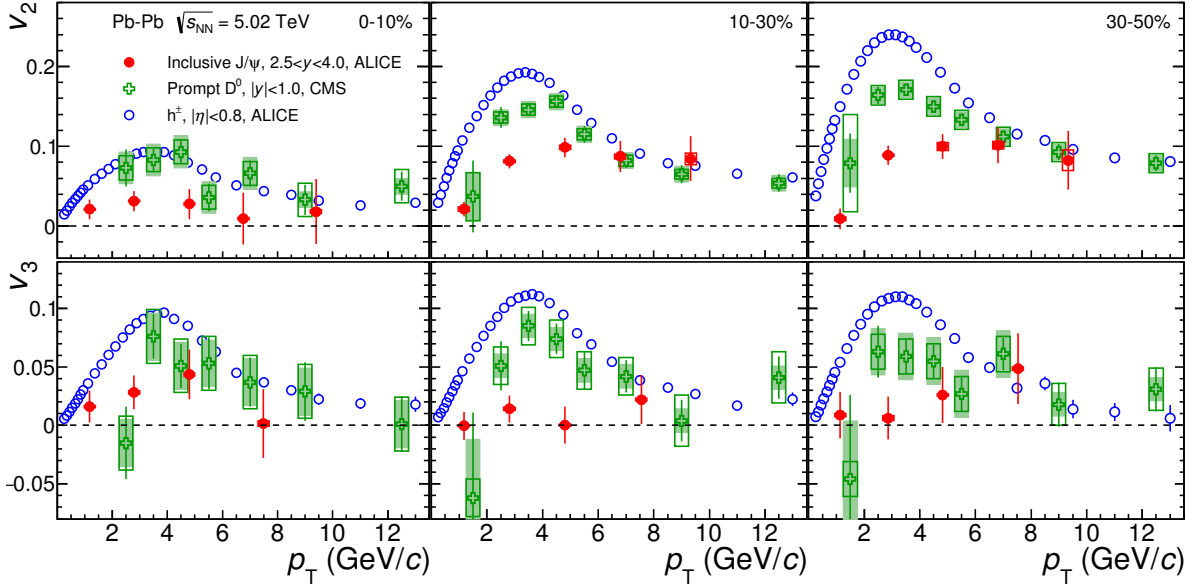


Fig. 4: (Color online) The J/ψ v_2 (upper panels) and v_3 (bottom panels) coefficients as a function of p_T in three centrality intervals (from left to right) in Pb–Pb collisions at $\sqrt{s_{NN}} = 5.02$ TeV. The results are compared to the v_2 and v_3 coefficients of mid-rapidity charged particles [50] and prompt D^0 mesons [23]. Statistical and systematic uncertainties are shown as bars and boxes, respectively. The shaded bands represent the systematic uncertainties from the contribution of non-prompt D^0 mesons.

$v_n(h^\pm)$ ($n = 2, 3$). At high p_T , above 6–8 GeV/c, the v_2 results indicate a convergence between charged particles, prompt D^0 mesons and J/ψ . Such an observation suggests that, at high p_T , the azimuthal asymmetry of the J/ψ mesons as well as that of charged particles and prompt D^0 mesons is possibly governed by in-medium path-length dependent energy-loss effects.

Discussing the above observations, should be noted the different rapidity interval of the J/ψ measurement. The effect of the decorrelation of the symmetry plane angles Ψ_n ($n = 2, 3$) between mid and forward pseudorapidity has been estimated to be less than 1% and 3% for v_2 and v_3 , respectively [51, 52]. An η dependence of the p_T -integrated v_n coefficients for charged particles has been observed in Pb–Pb collisions at $\sqrt{s_{NN}} = 2.76$ TeV [53]. However, the ratio v_3/v_2 has shown no significant dependence on η . Furthermore, the p_T -differential v_2 was found to be independent of η (up to $|\eta| < 2.4$) [54], thus indicating that the η dependence of the p_T -integrated v_2 arises mainly from changes in the transverse momentum spectra.

The presented results are for inclusive J/ψ and therefore the comparison to D^0 -meson results can be influenced by the considerable fraction of non-prompt J/ψ from b-hadron decays at intermediate and high transverse momentum [55, 56]. Finally, the J/ψ v_2 at intermediate and high transverse momentum can contain an additional contribution arising from a strong magnetic field at the initial stages of the collision, as suggested in Ref. [57].

The present analysis of the J/ψ v_2 coefficient, performed in the centrality intervals used in Ref. [19], yields consistent results. The main improvement with respect to the measurement in Ref. [19] is the up to 15% reduction of the statistical uncertainties due to the event-mixing approach described in Section 3.

In Fig. 4, the J/ψ v_3 is positive in most of the intervals, although it is also compatible with zero given the large uncertainties. A positive value of v_3 is found integrating the data over the centrality intervals, as seen in Fig. 5. The Fisher’s combined probability test [58] is used to quantify the probability that J/ψ v_3 is zero. The data in all p_T intervals are treated as independent measurements. The statistical and

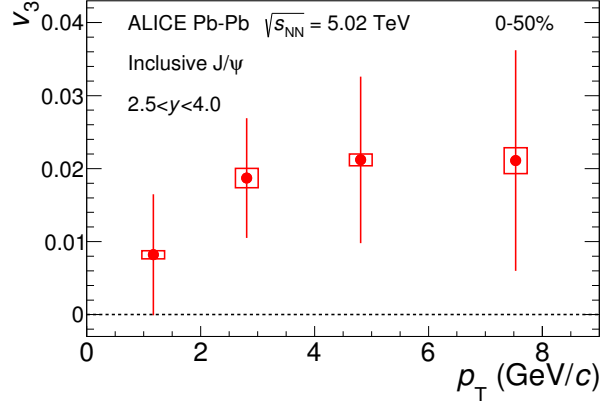


Fig. 5: (Color online) The J/ψ v_3 coefficient as a function of p_T in the 0–50% centrality interval in Pb–Pb collisions at $\sqrt{s_{NN}} = 5.02$ TeV. Statistical and systematic uncertainties are shown as bars and boxes, respectively.

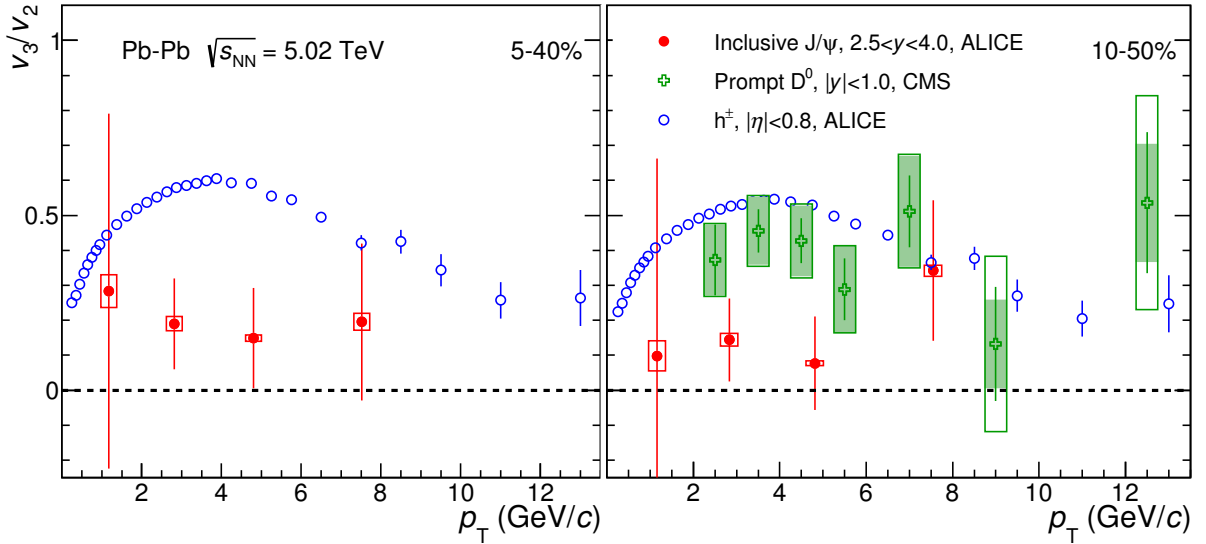


Fig. 6: (Color online) The J/ψ v_3/v_2 ratio as a function of p_T in the 5–40% (left panel) and 10–50% (right panel) centrality intervals in Pb–Pb collisions at $\sqrt{s_{NN}} = 5.02$ TeV. The results are compared to those of mid-rapidity charged particles [50] and prompt D^0 mesons [23]. Statistical and systematic uncertainties are shown as bars and boxes, respectively. The shaded bands represent the systematic uncertainties from the contribution of non-prompt D^0 mesons.

systematic uncertainties are added in quadrature. The total combined probability of the zero hypothesis is found to be 1.23×10^{-4} , which corresponds to about 3.7σ significance of the measured positive J/ψ v_3 coefficient.

The flow coefficients of the J/ψ , prompt D^0 mesons and charged particles are further compared in Fig. 6, where the ratio v_3/v_2 is shown as a function of p_T . In order to increase the significance of the ratio, the central collisions (0–5% and 0–10% centrality intervals), where v_2 has small magnitude, are excluded. The uncertainties of v_2 and v_3 coefficients are considered uncorrelated due to the weak correlation between the Ψ_2 and Ψ_3 angles [59]. Taking into account all p_T intervals, the obtained J/ψ v_3/v_2 ratio is found to be significantly lower (4.6σ) with respect to that of charged particles. Moreover, at intermediate p_T between 2 and 6 GeV/c, the prompt D^0 -mesons v_3/v_2 ratio is 2.3σ below that of charged particles and 3.4σ above that of the J/ψ mesons. Thus, the data seem to suggest an ordering similar to the one observed for the v_2 and v_3 coefficients in semi-central collisions. It is interesting to note that, in con-

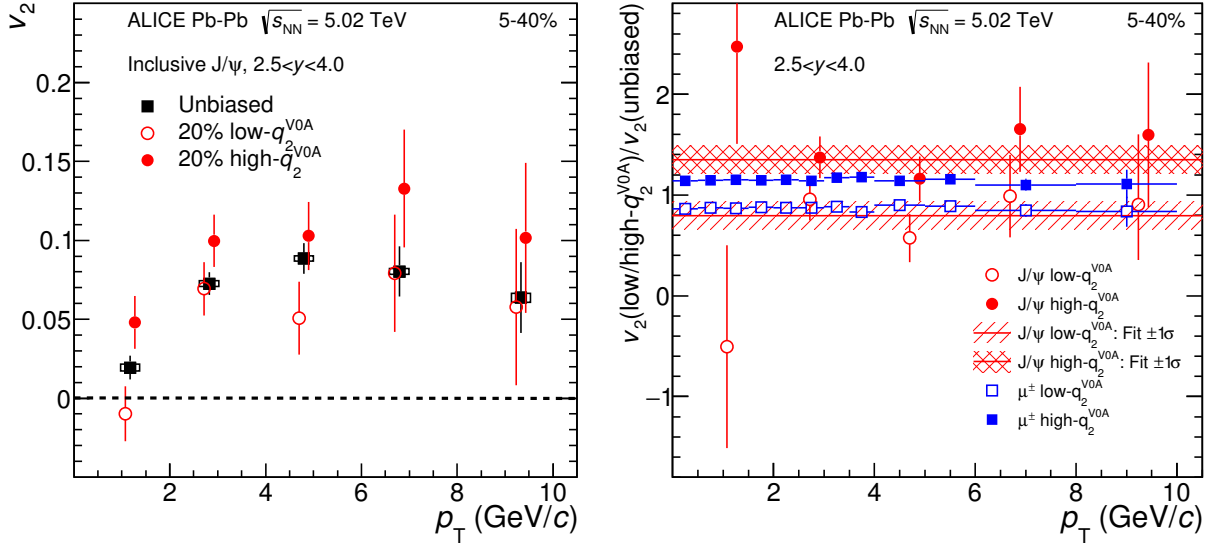


Fig. 7: (Color online) Left: The J/ψ v_2 as a function of p_T for shape selected and unbiased samples in the 5–40% centrality interval in Pb–Pb collisions at $\sqrt{s_{NN}} = 5.02$ TeV. Points are slightly shifted along the horizontal axis for better visibility. Statistical and systematic uncertainties are shown as bars and boxes, respectively. Right: Ratio of the J/ψ v_2 in lowest and highest q_2^{VOA} event-shape classes and the unbiased sample. The shaded bands represent the result with a constant function $\pm 1\sigma$. The J/ψ results are compared to the ratios for the single muons v_2 obtained with the same event-shape classes.

trast, the mass ordering of v_2 and v_3 seen for light-flavored particles is strongly suppressed in the ratio v_3/v_2 [27].

The left panel of Fig. 7 presents the J/ψ v_2 as a function of p_T for event-shape selected and unbiased events in the 5–40% centrality interval. The systematic uncertainties of the results from the event-shape selected and unbiased events are considered fully correlated and therefore cancel out in the ratios shown in the right panel of Fig. 7. The values of the J/ψ v_2 coefficient in low (high) q_2^{VOA} event classes are found to be lower (higher) with respect to those in the unbiased events. The v_2 coefficient of single muons is also measured in the same event-shape selected and unbiased samples. The corresponding ratios between the results in the event-shape selected and unbiased events show no p_T dependence up to 10 GeV/c (Fig. 7, right panel). This behavior demonstrates that the applied ESE technique based on q_2^{VOA} allows the selection of a global property of the collisions, most likely linked to the eccentricity ϵ_2 of the initial-state geometry [33]. The mean values of the ratios for single muons $v_2\{\text{low-}q_2^{VOA}\}/v_2\{\text{unbiased}\}$ and $v_2\{\text{high-}q_2^{VOA}\}/v_2\{\text{unbiased}\}$ are estimated from a fit with constant and are found to be 0.87 and 1.15, respectively. These values reflect the sensitivity of the VOA-based event-shape selection. The corresponding mean values of the J/ψ ratios, 0.79 ± 0.14 and 1.35 ± 0.14 , are consistent with the muon ratios. This implies that the J/ψ v_2 results are compatible with the expected variations of the eccentricity of the initial-state geometry within the uncertainties.

6 Conclusions

In summary, the elliptic and triangular flow coefficients of inclusive J/ψ mesons at forward rapidity have been measured in Pb–Pb collisions at $\sqrt{s_{NN}} = 5.02$ TeV over a broad range of transverse momentum and in various centrality intervals. This is the first measurement of the v_3 coefficient for inclusive J/ψ production, indicating a positive value with 3.7σ significance for $0 < p_T < 12$ GeV/c.

The obtained inclusive J/ψ v_2 and v_3 coefficients as well as the ratio v_3/v_2 are compared to the results for charged particles and prompt D^0 mesons at mid-rapidity. At low and intermediate p_T , the v_2 and v_3

results exhibit an ordering with the charged particles having largest values, followed by the prompt D^0 mesons and finally the J/ψ having the smallest values. In semi-central collisions at intermediate p_T , the J/ψ v_3/v_2 ratio is found to be significantly lower compared to that of charged particles. Despite the large uncertainties, the values of the prompt D^0 ratio are somewhat lower than the charged particles and higher than the J/ψ mesons, hinting at a possible ordering similar to that observed for the v_2 and v_3 coefficients.

At high p_T , the v_2 of the charged particles, the prompt D^0 mesons and the J/ψ seem to converge to similar values. The uncertainties of the v_3 coefficients do not allow one to draw firm conclusions about their convergence, although the centrality- and p_T -integrated J/ψ v_3 is compatible with that of high- p_T charged particles.

The analysis using Event Shape Engineering technique shows that the J/ψ v_2 coefficients increase (decrease) for classes of events with high (low) reduced event flow vector. Compared to single muons reconstructed in the same rapidity interval, the J/ψ results are found compatible with the expected variations of the eccentricity of the initial-state geometry.

Acknowledgements

The ALICE Collaboration would like to thank all its engineers and technicians for their invaluable contributions to the construction of the experiment and the CERN accelerator teams for the outstanding performance of the LHC complex. The ALICE Collaboration gratefully acknowledges the resources and support provided by all Grid centres and the Worldwide LHC Computing Grid (WLCG) collaboration. The ALICE Collaboration acknowledges the following funding agencies for their support in building and running the ALICE detector: A. I. Alikhanyan National Science Laboratory (Yerevan Physics Institute) Foundation (ANSL), State Committee of Science and World Federation of Scientists (WFS), Armenia; Austrian Academy of Sciences and Nationalstiftung für Forschung, Technologie und Entwicklung, Austria; Ministry of Communications and High Technologies, National Nuclear Research Center, Azerbaijan; Conselho Nacional de Desenvolvimento Científico e Tecnológico (CNPq), Universidade Federal do Rio Grande do Sul (UFRGS), Financiadora de Estudos e Projetos (Finep) and Fundação de Amparo à Pesquisa do Estado de São Paulo (FAPESP), Brazil; Ministry of Science & Technology of China (MSTC), National Natural Science Foundation of China (NSFC) and Ministry of Education of China (MOEC), China; Ministry of Science and Education, Croatia; Centro de Aplicaciones Tecnológicas y Desarrollo Nuclear (CEADEN), Cubaenergía, Cuba; Ministry of Education, Youth and Sports of the Czech Republic, Czech Republic; The Danish Council for Independent Research — Natural Sciences, the Carlsberg Foundation and Danish National Research Foundation (DNRF), Denmark; Helsinki Institute of Physics (HIP), Finland; Commissariat à l’Energie Atomique (CEA) and Institut National de Physique Nucléaire et de Physique des Particules (IN2P3) and Centre National de la Recherche Scientifique (CNRS), France; Bundesministerium für Bildung, Wissenschaft, Forschung und Technologie (BMBF) and GSI Helmholtzzentrum für Schwerionenforschung GmbH, Germany; General Secretariat for Research and Technology, Ministry of Education, Research and Religions, Greece; National Research, Development and Innovation Office, Hungary; Department of Atomic Energy Government of India (DAE), Department of Science and Technology, Government of India (DST), University Grants Commission, Government of India (UGC) and Council of Scientific and Industrial Research (CSIR), India; Indonesian Institute of Science, Indonesia; Centro Fermi - Museo Storico della Fisica e Centro Studi e Ricerche Enrico Fermi and Istituto Nazionale di Fisica Nucleare (INFN), Italy; Institute for Innovative Science and Technology, Nagasaki Institute of Applied Science (IIST), Japan Society for the Promotion of Science (JSPS) KAKENHI and Japanese Ministry of Education, Culture, Sports, Science and Technology (MEXT), Japan; Consejo Nacional de Ciencia (CONACYT) y Tecnología, through Fondo de Cooperación Internacional en Ciencia y Tecnología (FONCICYT) and Dirección General de Asuntos del Personal Académico (DGAPA), Mexico; Nederlandse Organisatie voor Wetenschappelijk Onderzoek (NWO), Netherlands; The Research Council of Norway, Norway; Commission on Science and Technol-

ogy for Sustainable Development in the South (COMSATS), Pakistan; Pontificia Universidad Católica del Perú, Peru; Ministry of Science and Higher Education and National Science Centre, Poland; Korea Institute of Science and Technology Information and National Research Foundation of Korea (NRF), Republic of Korea; Ministry of Education and Scientific Research, Institute of Atomic Physics and Romanian National Agency for Science, Technology and Innovation, Romania; Joint Institute for Nuclear Research (JINR), Ministry of Education and Science of the Russian Federation, National Research Centre Kurchatov Institute, Russian Science Foundation and Russian Foundation for Basic Research, Russia; Ministry of Education, Science, Research and Sport of the Slovak Republic, Slovakia; National Research Foundation of South Africa, South Africa; Swedish Research Council (VR) and Knut & Alice Wallenberg Foundation (KAW), Sweden; European Organization for Nuclear Research, Switzerland; National Science and Technology Development Agency (NSDTA), Suranaree University of Technology (SUT) and Office of the Higher Education Commission under NRU project of Thailand, Thailand; Turkish Atomic Energy Agency (TAEK), Turkey; National Academy of Sciences of Ukraine, Ukraine; Science and Technology Facilities Council (STFC), United Kingdom; National Science Foundation of the United States of America (NSF) and United States Department of Energy, Office of Nuclear Physics (DOE NP), United States of America.

References

- [1] J.-Y. Ollitrault, “Anisotropy as a signature of transverse collective flow,” *Phys. Rev. D* **46** (Jul, 1992) 229–245. <https://link.aps.org/doi/10.1103/PhysRevD.46.229>.
- [2] S. A. Voloshin, A. M. Poskanzer, and R. Snellings, “Collective phenomena in non-central nuclear collisions,” *Landolt-Bornstein* **23** (2010) 293–333, [arXiv:0809.2949](https://arxiv.org/abs/0809.2949) [nucl-ex].
- [3] S. Voloshin and Y. Zhang, “Flow study in relativistic nuclear collisions by Fourier expansion of Azimuthal particle distributions,” *Z. Phys.* **C70** (1996) 665–672, [arXiv:hep-ph/9407282](https://arxiv.org/abs/hep-ph/9407282) [hep-ph].
- [4] A. P. Mishra, R. K. Mohapatra, P. S. Saumia, and A. M. Srivastava, “Super-horizon fluctuations and acoustic oscillations in relativistic heavy-ion collisions,” *Phys. Rev.* **C77** (2008) 064902, [arXiv:0711.1323](https://arxiv.org/abs/0711.1323) [hep-ph].
- [5] J. Takahashi, B. M. Tavares, W. L. Qian, R. Andrade, F. Grassi, Y. Hama, T. Kodama, and N. Xu, “Topology studies of hydrodynamics using two particle correlation analysis,” *Phys. Rev. Lett.* **103** (2009) 242301, [arXiv:0902.4870](https://arxiv.org/abs/0902.4870) [nucl-th].
- [6] B. Alver and G. Roland, “Collision-geometry fluctuations and triangular flow in heavy-ion collisions,” *Phys. Rev. C* **81** (May, 2010) 054905. <https://link.aps.org/doi/10.1103/PhysRevC.81.054905>.
- [7] B. H. Alver, C. Gombeaud, M. Luzum, and J.-Y. Ollitrault, “Triangular flow in hydrodynamics and transport theory,” *Phys. Rev. C* **82** (Sep, 2010) 034913. <https://link.aps.org/doi/10.1103/PhysRevC.82.034913>.
- [8] D. Teaney and L. Yan, “Triangularity and Dipole Asymmetry in Heavy Ion Collisions,” *Phys. Rev.* **C83** (2011) 064904, [arXiv:1010.1876](https://arxiv.org/abs/1010.1876) [nucl-th].
- [9] ALICE Collaboration, B. Abelev *et al.*, “ J/ψ suppression at forward rapidity in Pb-Pb collisions at $\sqrt{s_{NN}} = 2.76$ TeV,” *Phys. Rev. Lett.* **109** (2012) 072301, [arXiv:1202.1383](https://arxiv.org/abs/1202.1383) [hep-ex].
- [10] ALICE Collaboration, B. B. Abelev *et al.*, “Centrality, rapidity and transverse momentum dependence of J/ψ suppression in Pb-Pb collisions at $\sqrt{s_{NN}}=2.76$ TeV,” *Phys. Lett.* **B734** (2014) 314–327, [arXiv:1311.0214](https://arxiv.org/abs/1311.0214) [nucl-ex].

- [11] ALICE Collaboration, J. Adam *et al.*, “ J/ψ suppression at forward rapidity in Pb-Pb collisions at $\sqrt{s_{NN}} = 5.02$ TeV,” *Phys. Lett.* **B766** (2017) 212–224, arXiv:1606.08197 [nucl-ex].
- [12] K. Zhou, N. Xu, Z. Xu, and P. Zhuang, “Medium effects on charmonium production at ultrarelativistic energies available at the CERN Large Hadron Collider,” *Phys. Rev.* **C89** no. 5, (2014) 054911, arXiv:1401.5845 [nucl-th].
- [13] X. Du and R. Rapp, “Sequential Regeneration of Charmonia in Heavy-Ion Collisions,” *Nucl. Phys.* **A943** (2015) 147–158, arXiv:1504.00670 [hep-ph].
- [14] M. He, R. J. Fries, and R. Rapp, “Heavy Flavor at the Large Hadron Collider in a Strong Coupling Approach,” *Phys. Lett.* **B735** (2014) 445–450, arXiv:1401.3817 [nucl-th].
- [15] P. Braun-Munzinger and J. Stachel, “(Non)thermal aspects of charmonium production and a new look at J/ψ suppression,” *Phys. Lett.* **B490** (2000) 196–202, arXiv:nucl-th/0007059 [nucl-th].
- [16] A. Andronic, P. Braun-Munzinger, K. Redlich, and J. Stachel, “The statistical model in Pb-Pb collisions at the LHC,” *Nucl. Phys.* **A904-905** (2013) 535c–538c, arXiv:1210.7724 [nucl-th].
- [17] ALICE Collaboration, J. Adam *et al.*, “Differential studies of inclusive J/ψ and $\psi(2S)$ production at forward rapidity in Pb-Pb collisions at $\sqrt{s_{NN}} = 2.76$ TeV,” *JHEP* **05** (2016) 179, arXiv:1506.08804 [nucl-ex].
- [18] A. Andronic, P. Braun-Munzinger, M. K. Koehler, and J. Stachel, “Testing charm quark thermalisation within the Statistical Hadronisation Model,” arXiv:1807.01236 [nucl-th].
- [19] ALICE Collaboration, S. Acharya *et al.*, “ J/ψ elliptic flow in Pb-Pb collisions at $\sqrt{s_{NN}} = 5.02$ TeV,” *Phys. Rev. Lett.* **119** no. 24, (2017) 242301, arXiv:1709.05260 [nucl-ex].
- [20] ALICE Collaboration, S. Acharya *et al.*, “Search for collectivity with azimuthal J/ψ -hadron correlations in high multiplicity p-Pb collisions at $\sqrt{s_{NN}} = 5.02$ and 8.16 TeV,” *Phys. Lett.* **B780** (2018) 7–20, arXiv:1709.06807 [nucl-ex].
- [21] CMS Collaboration, A. M. Sirunyan *et al.*, “Observation of prompt J/ψ meson elliptic flow in high-multiplicity pPb collisions at $\sqrt{s_{NN}} = 8.16$ TeV,” arXiv:1810.01473 [hep-ex].
- [22] X. Du and R. Rapp, “In-Medium Charmonium Production in Proton-Nucleus Collisions,” arXiv:1808.10014 [nucl-th].
- [23] CMS Collaboration, A. M. Sirunyan *et al.*, “Measurement of prompt D^0 meson azimuthal anisotropy in Pb-Pb collisions at $\sqrt{s_{NN}} = 5.02$ TeV,” *Phys. Rev. Lett.* **120** no. 20, (2018) 202301, arXiv:1708.03497 [nucl-ex].
- [24] ALICE Collaboration, S. Acharya *et al.*, “ D -meson azimuthal anisotropy in midcentral Pb-Pb collisions at $\sqrt{s_{NN}} = 5.02$ TeV,” *Phys. Rev. Lett.* **120** no. 10, (2018) 102301, arXiv:1707.01005 [nucl-ex].
- [25] F. G. Gardim, F. Grassi, M. Luzum, and J.-Y. Ollitrault, “Mapping the hydrodynamic response to the initial geometry in heavy-ion collisions,” *Phys. Rev.* **C85** (2012) 024908, arXiv:1111.6538 [nucl-th].
- [26] ALICE Collaboration, S. Acharya *et al.*, “Energy dependence and fluctuations of anisotropic flow in Pb-Pb collisions at $\sqrt{s_{NN}} = 5.02$ and 2.76 TeV,” *JHEP* **07** (2018) 103, arXiv:1804.02944 [nucl-ex].

- [27] ALICE Collaboration, S. Acharya *et al.*, “Anisotropic flow of identified particles in Pb-Pb collisions at $\sqrt{s_{NN}} = 5.02$ TeV,” *JHEP* **09** (2018) 006, arXiv:1805.04390 [nucl-ex].
- [28] R. J. Fries, V. Greco, and P. Sorensen, “Coalescence Models For Hadron Formation From Quark Gluon Plasma,” *Ann. Rev. Nucl. Part. Sci.* **58** (2008) 177–205, arXiv:0807.4939 [nucl-th].
- [29] B. Betz, M. Gyulassy, M. Luzum, J. Noronha, J. Noronha-Hostler, I. Portillo, and C. Ratti, “Cumulants and nonlinear response of high p_T harmonic flow at $\sqrt{s_{NN}} = 5.02$ TeV,” *Phys. Rev. C* **95** no. 4, (2017) 044901, arXiv:1609.05171 [nucl-th].
- [30] J. Schukraft, A. Timmins, and S. A. Voloshin, “Ultra-relativistic nuclear collisions: event shape engineering,” *Phys. Lett. B* **719** (2013) 394–398, arXiv:1208.4563 [nucl-ex].
- [31] ALICE Collaboration, B. Abelev *et al.*, “Anisotropic flow of charged hadrons, pions and (anti-)protons measured at high transverse momentum in Pb-Pb collisions at $\sqrt{s_{NN}}=2.76$ TeV,” *Phys. Lett. B* **719** (2013) 18–28, arXiv:1205.5761 [nucl-ex].
- [32] ATLAS Collaboration, G. Aad *et al.*, “Measurement of the correlation between flow harmonics of different order in lead-lead collisions at $\sqrt{s_{NN}}=2.76$ TeV with the ATLAS detector,” *Phys. Rev. C* **92** no. 3, (2015) 034903, arXiv:1504.01289 [hep-ex].
- [33] ALICE Collaboration, J. Adam *et al.*, “Event shape engineering for inclusive spectra and elliptic flow in Pb-Pb collisions at $\sqrt{s_{NN}} = 2.76$ TeV,” *Phys. Rev. C* **93** no. 3, (2016) 034916, arXiv:1507.06194 [nucl-ex].
- [34] ALICE Collaboration, S. Acharya *et al.*, “Event-shape engineering for the D-meson elliptic flow in mid-central Pb-Pb collisions at $\sqrt{s_{NN}} = 5.02$ TeV,” arXiv:1809.09371 [nucl-ex].
- [35] ALICE Collaboration, K. Aamodt *et al.*, “The ALICE experiment at the CERN LHC,” *JINST* **3** (2008) S08002.
- [36] ALICE Collaboration, B. Abelev *et al.*, “Performance of the ALICE Experiment at the CERN LHC,” *Int. J. Mod. Phys. A* **29** (2014) 1430044, arXiv:1402.4476 [nucl-ex].
- [37] ALICE Collaboration, K. Aamodt *et al.*, “Alignment of the ALICE Inner Tracking System with cosmic-ray tracks,” *JINST* **5** (2010) P03003, arXiv:1001.0502 [physics.ins-det].
- [38] ALICE Collaboration, J. Adam *et al.*, “Charged-particle multiplicities in proton-proton collisions at $\sqrt{s} = 0.9$ to 8 TeV,” *Eur. Phys. J. C* **77** no. 1, (2017) 33, arXiv:1509.07541 [nucl-ex].
- [39] ALICE Collaboration, E. Abbas *et al.*, “Performance of the ALICE VZERO system,” *JINST* **8** (2013) P10016, arXiv:1306.3130 [nucl-ex].
- [40] ALICE Collaboration, J. Adam *et al.*, “Centrality dependence of the charged-particle multiplicity density at midrapidity in Pb-Pb collisions at $\sqrt{s_{NN}} = 5.02$ TeV,” *Phys. Rev. Lett.* **116** no. 22, (2016) 222302, arXiv:1512.06104 [nucl-ex].
- [41] ALICE Collaboration, B. Abelev *et al.*, “Centrality determination of Pb-Pb collisions at $\sqrt{s_{NN}} = 2.76$ TeV with ALICE,” *Phys. Rev. C* **88** no. 4, (2013) 044909, arXiv:1301.4361 [nucl-ex].
- [42] STAR Collaboration, C. Adler *et al.*, “Elliptic flow from two and four particle correlations in Au+Au collisions at $\sqrt{s_{NN}} = 130$ GeV,” *Phys. Rev. C* **66** (2002) 034904, arXiv:nucl-ex/0206001 [nucl-ex].
- [43] I. Selyuzhenkov and S. Voloshin, “Effects of nonuniform acceptance in anisotropic flow measurements,” *Phys. Rev. C* **77** (2008) 034904.
<http://link.aps.org/doi/10.1103/PhysRevC.77.034904>.

- [44] N. Borghini and J. Y. Ollitrault, “Azimuthally sensitive correlations in nucleus-nucleus collisions,” *Phys. Rev.* **C70** (2004) 064905, arXiv:nucl-th/0407041 [nucl-th].
- [45] ALICE Collaboration, “Quarkonium signal extraction in ALICE,” <https://cds.cern.ch/record/2060096>. ALICE-PUBLIC-2015-006.
- [46] ALICE Collaboration, S. Acharya *et al.*, “Energy dependence of forward-rapidity J/ψ and $\psi(2S)$ production in pp collisions at the LHC,” *Eur. Phys. J.* **C77** no. 6, (2017) 392, arXiv:1702.00557 [hep-ex].
- [47] ALICE Collaboration, J. Adam *et al.*, “ ϕ -meson production at forward rapidity in p-Pb collisions at $\sqrt{s_{NN}} = 5.02$ TeV and in pp collisions at $\sqrt{s} = 2.76$ TeV,” *Phys. Lett.* **B768** (2017) 203–217, arXiv:1506.09206 [nucl-ex].
- [48] STAR Collaboration, L. Adamczyk *et al.*, “Measurements of Dielectron Production in Au+Au Collisions at $\sqrt{s_{NN}} = 200$ GeV from the STAR Experiment,” *Phys. Rev.* **C92** no. 2, (2015) 024912, arXiv:1504.01317 [hep-ex].
- [49] A. Bilandzic, C. H. Christensen, K. Gulbrandsen, A. Hansen, and Y. Zhou, “Generic framework for anisotropic flow analyses with multiparticle azimuthal correlations,” *Phys. Rev.* **C89** no. 6, (2014) 064904, arXiv:1312.3572 [nucl-ex].
- [50] ALICE Collaboration, S. Acharya *et al.*, “Energy dependence and fluctuations of anisotropic flow in Pb-Pb collisions at $\sqrt{s_{NN}} = 5.02$ and 2.76 TeV,” arXiv:1804.02944 [nucl-ex].
- [51] CMS Collaboration, V. Khachatryan *et al.*, “Evidence for transverse momentum and pseudorapidity dependent event plane fluctuations in PbPb and pPb collisions,” *Phys. Rev.* **C92** no. 3, (2015) 034911, arXiv:1503.01692 [nucl-ex].
- [52] ATLAS Collaboration, M. Aaboud *et al.*, “Measurement of longitudinal flow decorrelations in Pb+Pb collisions at $\sqrt{s_{NN}} = 2.76$ and 5.02 TeV with the ATLAS detector,” *Eur. Phys. J.* **C78** no. 2, (2018) 142, arXiv:1709.02301 [nucl-ex].
- [53] ALICE Collaboration, J. Adam *et al.*, “Pseudorapidity dependence of the anisotropic flow of charged particles in Pb-Pb collisions at $\sqrt{s_{NN}} = 2.76$ TeV,” *Phys. Lett.* **B762** (2016) 376–388, arXiv:1605.02035 [nucl-ex].
- [54] CMS Collaboration, S. Chatrchyan *et al.*, “Measurement of the elliptic anisotropy of charged particles produced in PbPb collisions at $\sqrt{s_{NN}} = 2.76$ TeV,” *Phys. Rev.* **C87** no. 1, (2013) 014902, arXiv:1204.1409 [nucl-ex].
- [55] ALICE Collaboration, J. Adam *et al.*, “Inclusive, prompt and non-prompt J/ψ production at mid-rapidity in Pb-Pb collisions at $\sqrt{s_{NN}} = 2.76$ TeV,” *JHEP* **07** (2015) 051, arXiv:1504.07151 [nucl-ex].
- [56] CMS Collaboration, S. Chatrchyan *et al.*, “Suppression of non-prompt J/ψ , prompt J/ψ , and $Y(1S)$ in PbPb collisions at $\sqrt{s_{NN}} = 2.76$ TeV,” *JHEP* **05** (2012) 063, arXiv:1201.5069 [nucl-ex].
- [57] X. Guo, S. Shi, N. Xu, Z. Xu, and P. Zhuang, “Magnetic Field Effect on Charmonium Production in High Energy Nuclear Collisions,” *Phys. Lett.* **B751** (2015) 215–219, arXiv:1502.04407 [hep-ph].
- [58] R. A. Fisher, *Statistical Methods for Research Workers*, pp. 66–70. Springer New York, New York, NY, 1992. http://dx.doi.org/10.1007/978-1-4612-4380-9_6.

- [59] **ATLAS** Collaboration, G. Aad *et al.*, “Measurement of event-plane correlations in $\sqrt{s_{NN}} = 2.76$ TeV lead-lead collisions with the ATLAS detector,” *Phys. Rev.* **C90** no. 2, (2014) 024905, arXiv:1403.0489 [hep-ex].

A Appendix

The azimuthal distribution of the combinatorial background $dN^B/d\varphi$ is a product of the azimuthal distributions of the single muons from which the background dimuons are formed. Thus, using Eq.(1) one obtains

$$\begin{aligned} \frac{dN^B}{d\varphi} &\propto (1 + 2 \sum_{n=1}^{\infty} v_n^{(1)}(p_T^{(1)}, \eta_1) \cos[n(\varphi_1 - \Psi_n)]) (1 + 2 \sum_{m=1}^{\infty} v_m^{(2)}(p_T^{(2)}, \eta_2) \cos[m(\varphi_2 - \Psi_m)]) \\ &\propto 1 + 2 \sum_{n=1}^{\infty} v_n^{(1)}(p_T^{(1)}, \eta_1) \cos[n(\Delta\varphi_1 + \varphi - \Psi_n)] \\ &\quad + 2 \sum_{m=1}^{\infty} v_m^{(2)}(p_T^{(2)}, \eta_2) \cos[m(\Delta\varphi_2 + \varphi - \Psi_m)] \\ &\quad + 4 \sum_{n=1}^{\infty} \sum_{m=1}^{\infty} v_n^{(1)}(p_T^{(1)}, \eta_1) v_m^{(2)}(p_T^{(2)}, \eta_2) \cos[n(\Delta\varphi_1 + \varphi - \Psi_n)] \cos[m(\Delta\varphi_2 + \varphi - \Psi_m)], \end{aligned} \quad (\text{A.1})$$

where $v_n^{(1)}(p_T^{(1)}, \eta_1)$ and $v_m^{(2)}(p_T^{(2)}, \eta_2)$ are the flow coefficients of the two muons as a function of their transverse momenta and pseudorapidities, φ_1 and φ_2 are the azimuthal angles of the two muons, φ is the azimuthal angle of the dimuon and $\Delta\varphi_{1,2} = \varphi_{1,2} - \varphi$.

The n -th order flow coefficient of the background dimuon is then calculated as

$$v_n^B(p_T^{(1)}, p_T^{(2)}, \eta_1, \eta_2, \varphi_1, \varphi_2) = \langle \cos[n(\varphi - \Psi_n)] \rangle = \frac{\int_0^{2\pi} \frac{dN^B}{d\varphi} \cos[n(\varphi - \Psi_n)] d\varphi}{\int_0^{2\pi} \frac{dN^B}{d\varphi} d\varphi}. \quad (\text{A.2})$$

The denominator in Eq.(A.2) is obtained as

$$\begin{aligned} &2\pi + 2 \sum_{n=1}^{\infty} v_n^{(1)}(p_T^{(1)}, \eta_1) I_n(\Delta\varphi_1) + 2 \sum_{m=1}^{\infty} v_m^{(2)}(p_T^{(2)}, \eta_2) I_m(\Delta\varphi_2) \\ &+ 4 \sum_{n=1}^{\infty} \sum_{m=1}^{\infty} v_n^{(1)}(p_T^{(1)}, \eta_1) v_m^{(2)}(p_T^{(2)}, \eta_2) I_{nm}(\Delta\varphi_1, \Delta\varphi_2), \end{aligned} \quad (\text{A.3})$$

where

$$I_n(\Delta\varphi_{1,2}) = \int_0^{2\pi} \cos[n(\Delta\varphi_{1,2} + \varphi - \Psi_n)] d\varphi = 0, \quad (\text{A.4})$$

$$I_{mn}(\Delta\varphi_1, \Delta\varphi_2) = \int_0^{2\pi} \cos[n(\Delta\varphi_1 + \varphi - \Psi_n)] \cos[m(\Delta\varphi_2 + \varphi - \Psi_m)] d\varphi = \begin{cases} 0, & n \neq m \\ \pi \cos[n(\Delta\varphi_1 - \Delta\varphi_2)], & n = m. \end{cases} \quad (\text{A.5})$$

The numerator in Eq.(A.2) is obtained as

$$\begin{aligned} &2 \sum_{k=1}^{\infty} v_k^{(1)}(p_T^{(1)}, \eta_1) J_{kn}(\Delta\varphi_1) + 2 \sum_{m=1}^{\infty} v_m^{(2)}(p_T^{(2)}, \eta_2) J_{mn}(\Delta\varphi_2) \\ &+ 4 \sum_{k=1}^{\infty} \sum_{m=1}^{\infty} v_k^{(1)}(p_T^{(1)}, \eta_1) v_m^{(2)}(p_T^{(2)}, \eta_2) J_{kmn}(\Delta\varphi_1, \Delta\varphi_2), \end{aligned} \quad (\text{A.6})$$

where

$$J_{kn}(\Delta\varphi_{1,2}) = \int_0^{2\pi} \cos[k(\Delta\varphi_{1,2} + \varphi - \Psi_k)] \cos[n(\varphi - \Psi_n)] d\varphi = \begin{cases} 0, & k \neq n \\ \pi \cos[n\Delta\varphi_{1,2}], & k = n, \end{cases} \quad (\text{A.7})$$

$$J_{kmn}(\Delta\varphi_1, \Delta\varphi_2) = \int_0^{2\pi} \cos[k(\Delta\varphi_1 + \varphi - \Psi_k)] \cos[m(\Delta\varphi_2 + \varphi - \Psi_m)] \cos[n(\varphi - \Psi_n)] d\varphi = 0. \quad (\text{A.8})$$

Combining Eq.(A.2)-(A.8) yields

$$v_n^B(p_T^{(1)}, p_T^{(2)}, \eta_1, \eta_2, \varphi_1, \varphi_2) = \frac{v_n^{(1)}(p_T^{(1)}, \eta_1) \cos[n(\varphi_1 - \varphi)] + v_n^{(2)}(p_T^{(2)}, \eta_2) \cos[n(\varphi_2 - \varphi)]}{1 + 2 \sum_{m=1}^{\infty} v_m^{(1)}(p_T^{(1)}, \eta_1) v_m^{(2)}(p_T^{(2)}, \eta_2) \cos[m(\varphi_1 - \varphi_2)]}. \quad (\text{A.9})$$

Finally, the v_n^B as a function of $M_{\mu\mu}$ is obtained by averaging the numerator and denominator in Eq.(A.9) over all dimuons, which belong to a given $M_{\mu\mu}$ interval:

$$v_n^B(M_{\mu\mu}) = \frac{\langle v_n^{(1)}(p_T^{(1)}, \eta_1) \cos[n(\varphi_1 - \varphi)] + v_n^{(2)}(p_T^{(2)}, \eta_2) \cos[n(\varphi_2 - \varphi)] \rangle_{M_{\mu\mu}}}{\langle 1 + 2 \sum_{m=1}^{\infty} v_m^{(1)}(p_T^{(1)}, \eta_1) v_m^{(2)}(p_T^{(2)}, \eta_2) \cos[m(\varphi_1 - \varphi_2)] \rangle_{M_{\mu\mu}}}. \quad (\text{A.10})$$

The Eq.(A.8) is derived assuming no correlation between different harmonic symmetry plane angles Ψ . While this is in general the case, there are some noticeable exceptions [59]. In fact, the significant correlation between the Ψ_2 and Ψ_4 angles leads to non-zero J_{422} . The corresponding contribution to the numerator of Eq.(A.10) for v_2^B is given approximately by

$$\begin{aligned} & \frac{1}{2} \langle \cos[4(\Psi_4 - \Psi_2)] \rangle \langle v_4^{(1)}(p_T^{(1)}, \eta_1) v_2^{(2)}(p_T^{(2)}, \eta_2) \cos[4(\varphi_1 - \varphi) - 2(\varphi_2 - \varphi)] \\ & + v_4^{(2)}(p_T^{(2)}, \eta_2) v_2^{(1)}(p_T^{(1)}, \eta_1) \cos[4(\varphi_2 - \varphi) - 2(\varphi_1 - \varphi)] \rangle_{M_{\mu\mu}}, \end{aligned} \quad (\text{A.11})$$

where the brackets $\langle \dots \rangle$ denote an average over all events. The contribution is estimated as described in the following. First, the v_2 and v_4 coefficients of single muons are measured with the SP method, averaged over pseudorapidity and parameterized as a function of p_T . The obtained parameterizations $v_{2,4}(p_T)$ are then combined with opposite-sign dimuons $(p_T^{(1)}, p_T^{(2)}, \eta_1, \eta_2, \varphi_1, \varphi_2)$ in the data outside the J/ψ mass peak. The values of $\langle \cos[4(\Psi_4 - \Psi_2)] \rangle$, which ranges from 0 in central collisions to about 0.8 in peripheral collisions, are taken from Ref. [59]. Finally, the magnitude of the effect is calculated via interpolation of the results at the J/ψ mass peak. In general, the magnitude is found to be at the order of 10^{-4} , reaching at most 7×10^{-4} for $0 < p_T < 2$ GeV/c and the 30–50% centrality interval.

A similar effect is present in the numerator of Eq.(A.10) for v_3^B , due to the correlation of the Ψ_3 and Ψ_6 angles. In practice, however, this contribution can be certainly neglected, because of the small magnitude of the v_6 coefficient.

B The ALICE Collaboration

S. Acharya¹³⁹, F.T.-. Acosta²⁰, D. Adamová⁹³, A. Adler⁷⁴, J. Adolfsson⁸⁰, M.M. Aggarwal⁹⁸, G. Aglieri Rinella³⁴, M. Agnello³¹, N. Agrawal⁴⁸, Z. Ahammed¹³⁹, S.U. Ahn⁷⁶, S. Aiola¹⁴⁴, A. Akindinov⁶⁴, M. Al-Turany¹⁰⁴, S.N. Alam¹³⁹, D.S.D. Albuquerque¹²¹, D. Aleksandrov⁸⁷, B. Alessandro⁵⁸, H.M. Alfanda⁶, R. Alfaro Molina⁷², Y. Ali¹⁵, A. Alici^{10,27,53}, A. Alkin², J. Alme²², T. Alt⁶⁹, L. Altenkamper²², I. Altsybeev¹¹¹, M.N. Anaam⁶, C. Andrei⁴⁷, D. Andreou³⁴, H.A. Andrews¹⁰⁸, A. Andronic^{142,104}, M. Angeletti³⁴, V. Anguelov¹⁰², C. Anson¹⁶, T. Antičić¹⁰⁵, F. Antinori⁵⁶, P. Antonioli⁵³, R. Anwar¹²⁵, N. Apadula⁷⁹, L. Aphecetche¹¹³, H. Appelshäuser⁶⁹, S. Arcelli²⁷, R. Arnaldi⁵⁸, I.C. Arsene²¹, M. Arslandok¹⁰², A. Augustinus³⁴, R. Averbek¹⁰⁴, M.D. Azmi¹⁷, A. Badalá⁵⁵, Y.W. Baek^{60,40}, S. Bagnasco⁵⁸, R. Bailhache⁶⁹, R. Bala⁹⁹, A. Baldisseri¹³⁵, M. Ball⁴², R.C. Baral⁸⁵, A.M. Barbano²⁶, R. Barbera²⁸, F. Barile⁵², L. Barioglio²⁶, G.G. Barnaföldi¹⁴³, L.S. Barnby⁹², V. Barret¹³², P. Bartalini⁶, K. Barth³⁴, E. Bartsch⁶⁹, N. Bastid¹³², S. Basu¹⁴¹, G. Batigne¹¹³, B. Batyunya⁷⁵, P.C. Batzing²¹, J.L. Bazo Alba¹⁰⁹, I.G. Bearden⁸⁸, H. Beck¹⁰², C. Bedda⁶³, N.K. Behera⁶⁰, I. Belikov¹³⁴, F. Bellini³⁴, H. Bello Martinez⁴⁴, R. Bellwied¹²⁵, L.G.E. Beltran¹¹⁹, V. Belyaev⁹¹, G. Bencedi¹⁴³, S. Beole²⁶, A. Bercuci⁴⁷, Y. Berdnikov⁹⁶, D. Berenyi¹⁴³, R.A. Bertens¹²⁸, D. Berzano^{58,34}, L. Betev³⁴, P.P. Bhaduri¹³⁹, A. Bhasin⁹⁹, I.R. Bhat⁹⁹, H. Bhatt⁴⁸, B. Bhattacharjee⁴¹, J. Bhom¹¹⁷, A. Bianchi²⁶, L. Bianchi¹²⁵, N. Bianchi⁵¹, J. Bielčik³⁷, J. Bielčiková⁹³, A. Bilandzic^{103,116}, G. Biro¹⁴³, R. Biswas³, S. Biswas³, J.T. Blair¹¹⁸, D. Blau⁸⁷, C. Blume⁶⁹, G. Boca¹³⁷, F. Bock³⁴, A. Bogdanov⁹¹, L. Boldizsár¹⁴³, A. Bolozdynya⁹¹, M. Bombara³⁸, G. Bonomi¹³⁸, M. Bonora³⁴, H. Borel¹³⁵, A. Borissov^{142,102}, M. Borri¹²⁷, E. Botta²⁶, C. Bourjau⁸⁸, L. Bratrud⁶⁹, P. Braun-Munzinger¹⁰⁴, M. Bregant¹²⁰, T.A. Broker⁶⁹, M. Broz³⁷, E.J. Brucken⁴³, E. Bruna⁵⁸, G.E. Bruno^{34,33}, D. Budnikov¹⁰⁶, H. Buesching⁶⁹, S. Bufalino³¹, P. Buhler¹¹², P. Buncic³⁴, O. Busch^{131,i}, Z. Buthelezi⁷³, J.B. Butt¹⁵, J.T. Buxton⁹⁵, J. Cabala¹¹⁵, D. Caffarri⁸⁹, H. Caines¹⁴⁴, A. Caliva¹⁰⁴, E. Calvo Villar¹⁰⁹, R.S. Camacho⁴⁴, P. Camerini²⁵, A.A. Capon¹¹², W. Carena³⁴, F. Carnesecchi^{10,27}, J. Castillo Castellanos¹³⁵, A.J. Castro¹²⁸, E.A.R. Casula⁵⁴, C. Ceballos Sanchez⁸, S. Chandra¹³⁹, B. Chang¹²⁶, W. Chang⁶, S. Chapeland³⁴, M. Chartier¹²⁷, S. Chattopadhyay¹³⁹, S. Chattopadhyay¹⁰⁷, A. Chauvin²⁴, C. Cheshkov¹³³, B. Cheynis¹³³, V. Chibante Barroso³⁴, D.D. Chinellato¹²¹, S. Cho⁶⁰, P. Chochula³⁴, T. Chowdhury¹³², P. Christakoglou⁸⁹, C.H. Christensen⁸⁸, P. Christiansen⁸⁰, T. Chujo¹³¹, S.U. Chung¹⁸, C. Cicalo⁵⁴, L. Cifarelli^{10,27}, F. Cindolo⁵³, J. Cleymans¹²⁴, F. Colamaria⁵², D. Colella⁵², A. Collu⁷⁹, M. Colocci²⁷, M. Concas^{58,ii}, G. Conesa Balbastre⁷⁸, Z. Conesa del Valle⁶¹, J.G. Contreras³⁷, T.M. Cormier⁹⁴, Y. Corrales Morales⁵⁸, P. Cortese³², M.R. Cosentino¹²², F. Costa³⁴, S. Costanza¹³⁷, J. Crkovská⁶¹, P. Crochet¹³², E. Cuautle⁷⁰, L. Cunqueiro^{94,142}, T. Dahms^{103,116}, A. Dainese⁵⁶, F.P.A. Damas^{113,135}, S. Dani⁶⁶, M.C. Danisch¹⁰², A. Danu⁶⁸, D. Das¹⁰⁷, I. Das¹⁰⁷, S. Das³, A. Dash⁸⁵, S. Dash⁴⁸, S. De⁴⁹, A. De Caro³⁰, G. de Cataldo⁵², C. de Conti¹²⁰, J. de Cuveland³⁹, A. De Falco²⁴, D. De Gruttola^{10,30}, N. De Marco⁵⁸, S. De Pasquale³⁰, R.D. De Souza¹²¹, H.F. Degenhardt¹²⁰, A. Deisting^{104,102}, A. Deloff⁸⁴, S. Delsanto²⁶, C. Deplano⁸⁹, P. Dhankher⁴⁸, D. Di Bari³³, A. Di Mauro³⁴, B. Di Ruzza⁵⁶, R.A. Diaz⁸, T. Dietel¹²⁴, P. Dillenseger⁶⁹, Y. Ding⁶, R. Diviã³⁴, Ø. Djuvsland²², A. Dobrin³⁴, D. Domenicis Gimenez¹²⁰, B. Dönigus⁶⁹, O. Dordic²¹, A.K. Dubey¹³⁹, A. Dubla¹⁰⁴, L. Ducroux¹³³, S. Dudi⁹⁸, A.K. Duggal⁹⁸, M. Dukhishyam⁸⁵, P. Dupieux¹³², R.J. Ehlers¹⁴⁴, D. Elia⁵², E. Endress¹⁰⁹, H. Engel⁷⁴, E. Epple¹⁴⁴, B. Erasmus¹¹³, F. Erhardt⁹⁷, M.R. Ersdal²², B. Espagnon⁶¹, G. Eulisse³⁴, J. Eum¹⁸, D. Evans¹⁰⁸, S. Evdokimov⁹⁰, L. Fabbietti^{103,116}, M. Faggin²⁹, J. Faivre⁷⁸, A. Fantoni⁵¹, M. Fasel⁹⁴, L. Feldkamp¹⁴², A. Feliciello⁵⁸, G. Feofilov¹¹¹, A. Fernández Téllez⁴⁴, A. Ferretti²⁶, A. Festanti³⁴, V.J.G. Feuillard¹⁰², J. Figiel¹¹⁷, M.A.S. Figueredo¹²⁰, S. Filchagin¹⁰⁶, D. Finogeev⁶², F.M. Fionda²², G. Fiorenza⁵², F. Flor¹²⁵, M. Floris³⁴, S. Foertsch⁷³, P. Foka¹⁰⁴, S. Fokin⁸⁷, E. Fragiaco⁵⁹, A. Francescon³⁴, A. Francisco¹¹³, U. Frankenfeld¹⁰⁴, G.G. Fronze²⁶, U. Fuchs³⁴, C. Furget⁷⁸, A. Furs⁶², M. Fusco Girard³⁰, J.J. Gaardhøje⁸⁸, M. Gagliardi²⁶, A.M. Gago¹⁰⁹, K. Gajdosova⁸⁸, M. Gallio²⁶, C.D. Galvan¹¹⁹, P. Ganoti⁸³, C. Garabatos¹⁰⁴, E. Garcia-Solis¹¹, K. Garg²⁸, C. Gargiulo³⁴, P. Gasik^{116,103}, E.F. Gauger¹¹⁸, M.B. Gay Ducati⁷¹, M. Germain¹¹³, J. Ghosh¹⁰⁷, P. Ghosh¹³⁹, S.K. Ghosh³, P. Gianotti⁵¹, P. Giubellino^{104,58}, P. Giubileo²⁹, P. Glässel¹⁰², D.M. Gómez Coral⁷², A. Gomez Ramirez⁷⁴, V. Gonzalez¹⁰⁴, P. González-Zamora⁴⁴, S. Gorbunov³⁹, L. Görlich¹¹⁷, S. Gotovac³⁵, V. Grabski⁷², L.K. Graczykowski¹⁴⁰, K.L. Graham¹⁰⁸, L. Greiner⁷⁹, A. Grelli⁶³, C. Grigoras³⁴, V. Grigoriev⁹¹, A. Grigoryan¹, S. Grigoryan⁷⁵, J.M. Gronefeld¹⁰⁴, F. Grosa³¹, J.F. Grosse-Oetringhaus³⁴, R. Grosso¹⁰⁴, R. Guernane⁷⁸, B. Guerzoni²⁷, M. Guittiere¹¹³, K. Gulbrandsen⁸⁸, T. Gunji¹³⁰, A. Gupta⁹⁹, R. Gupta⁹⁹, I.B. Guzman⁴⁴, R. Haake^{34,144}, M.K. Habib¹⁰⁴, C. Hadjidakis⁶¹, H. Hamagaki⁸¹, G. Hamar¹⁴³, M. Hamid⁶, J.C. Hamon¹³⁴, R. Hannigan¹¹⁸, M.R. Haque⁶³, A. Harlanderova¹⁰⁴, J.W. Harris¹⁴⁴, A. Harton¹¹, H. Hassan⁷⁸, D. Hatzifotiadou^{53,10}, S. Hayashi¹³⁰, S.T. Heckel⁶⁹, E. Hellbär⁶⁹, H. Helstrup³⁶, A. Hergehelegiu⁴⁷, E.G. Hernandez⁴⁴, G. Herrera Corral⁹, F. Herrmann¹⁴², K.F. Hetland³⁶, T.E. Hilden⁴³, H. Hillemanns³⁴, C. Hills¹²⁷, B. Hippolyte¹³⁴, B. Hohlweger¹⁰³, D. Horak³⁷, S. Hornung¹⁰⁴, R. Hosokawa^{131,78}, J. Hota⁶⁶,

P. Hristov³⁴, C. Huang⁶¹, C. Hughes¹²⁸, P. Huhn⁶⁹, T.J. Humanic⁹⁵, H. Hushnud¹⁰⁷, N. Hussain⁴¹, T. Hussain¹⁷, D. Hutter³⁹, D.S. Hwang¹⁹, J.P. Iddon¹²⁷, R. Ilkaev¹⁰⁶, M. Inaba¹³¹, M. Ippolitov⁸⁷, M.S. Islam¹⁰⁷, M. Ivanov¹⁰⁴, V. Ivanov⁹⁶, V. Izucheev⁹⁰, B. Jacak⁷⁹, N. Jacazio²⁷, P.M. Jacobs⁷⁹, M.B. Jadhav⁴⁸, S. Jadlovská¹¹⁵, J. Jadlovsky¹¹⁵, S. Jaelani⁶³, C. Jahnke^{120,116}, M.J. Jakubowska¹⁴⁰, M.A. Janik¹⁴⁰, C. Jena⁸⁵, M. Jercic⁹⁷, O. Jevons¹⁰⁸, R.T. Jimenez Bustamante¹⁰⁴, M. Jin¹²⁵, P.G. Jones¹⁰⁸, A. Jusko¹⁰⁸, P. Kalinak⁶⁵, A. Kalweit³⁴, J.H. Kang¹⁴⁵, V. Kaplin⁹¹, S. Kar⁶, A. Karasu Uysal⁷⁷, O. Karavichev⁶², T. Karavicheva⁶², P. Karczmarczyk³⁴, E. Karpechev⁶², U. Keschull⁷⁴, R. Keidel⁴⁶, D.L.D. Keijdener⁶³, M. Keil³⁴, B. Ketzer⁴², Z. Khabanova⁸⁹, A.M. Khan⁶, S. Khan¹⁷, S.A. Khan¹³⁹, A. Khanzadeev⁹⁶, Y. Kharlov⁹⁰, A. Khatun¹⁷, A. Khuntia⁴⁹, M.M. Kielbowicz¹¹⁷, B. Kileng³⁶, B. Kim¹³¹, D. Kim¹⁴⁵, D.J. Kim¹²⁶, E.J. Kim¹³, H. Kim¹⁴⁵, J.S. Kim⁴⁰, J. Kim¹⁰², J. Kim¹³, M. Kim^{60,102}, S. Kim¹⁹, T. Kim¹⁴⁵, T. Kim¹⁴⁵, K. Kindra⁹⁸, S. Kirsch³⁹, I. Kisel³⁹, S. Kiselev⁶⁴, A. Kisiel¹⁴⁰, J.L. Klay⁵, C. Klein⁶⁹, J. Klein⁵⁸, C. Klein-Bösing¹⁴², S. Klewin¹⁰², A. Kluge³⁴, M.L. Knichel³⁴, A.G. Knospe¹²⁵, C. Kobdaj¹¹⁴, M. Kofarago¹⁴³, M.K. Köhler¹⁰², T. Kollegger¹⁰⁴, N. Kondratyeva⁹¹, E. Kondratyuk⁹⁰, A. Konevskikh⁶², P.J. Konopka³⁴, M. Konyushikhin¹⁴¹, L. Koska¹¹⁵, O. Kovalenko⁸⁴, V. Kovalenko¹¹¹, M. Kowalski¹¹⁷, I. Králik⁶⁵, A. Kravčáková³⁸, L. Kreis¹⁰⁴, M. Krivda^{65,108}, F. Krizek⁹³, M. Krüger⁶⁹, E. Kryshen⁹⁶, M. Krzewicki³⁹, A.M. Kubera⁹⁵, V. Kučera^{93,60}, C. Kuhn¹³⁴, P.G. Kuijper⁸⁹, J. Kumar⁴⁸, L. Kumar⁹⁸, S. Kumar⁴⁸, S. Kundu⁸⁵, P. Kurashvili⁸⁴, A. Kurepin⁶², A.B. Kurepin⁶², S. Kushpil⁹³, J. Kvapil¹⁰⁸, M.J. Kweon⁶⁰, Y. Kwon¹⁴⁵, S.L. La Pointe³⁹, P. La Rocca²⁸, Y.S. Lai⁷⁹, I. Lakomov³⁴, R. Langoy¹²³, K. Lapidus¹⁴⁴, A. Lardeux²¹, P. Larionov⁵¹, E. Laudi³⁴, R. Lavicka³⁷, R. Lea²⁵, L. Leardini¹⁰², S. Lee¹⁴⁵, F. Lehas⁸⁹, S. Lehner¹¹², J. Lehrbach³⁹, R.C. Lemmon⁹², I. León Monzón¹¹⁹, P. Lévai¹⁴³, X. Li¹², X.L. Li⁶, J. Lien¹²³, R. Lietava¹⁰⁸, B. Lim¹⁸, S. Lindal²¹, V. Lindenstruth³⁹, S.W. Lindsay¹²⁷, C. Lippmann¹⁰⁴, M.A. Lisa⁹⁵, V. Litichevskyi⁴³, A. Liu⁷⁹, H.M. Ljunggren⁸⁰, W.J. Llope¹⁴¹, D.F. Lodato⁶³, V. Loginov⁹¹, C. Loizides^{94,79}, P. Loncar³⁵, X. Lopez¹³², E. López Torres⁸, P. Luettig⁶⁹, J.R. Luhder¹⁴², M. Lunardon²⁹, G. Luparello⁵⁹, M. Lupi³⁴, A. Maevskaya⁶², M. Mager³⁴, S.M. Mahmood²¹, A. Maire¹³⁴, R.D. Majka¹⁴⁴, M. Malaev⁹⁶, Q.W. Malik²¹, L. Malinina^{75,iii}, D. Mal'Kevich⁶⁴, P. Malzacher¹⁰⁴, A. Mamonov¹⁰⁶, V. Manko⁸⁷, F. Manso¹³², V. Manzari⁵², Y. Mao⁶, M. Marchisone^{133,129}, J. Mareš⁶⁷, G.V. Margagliotti²⁵, A. Margotti⁵³, J. Margutti⁶³, A. Marín¹⁰⁴, C. Markert¹¹⁸, M. Marquard⁶⁹, N.A. Martin^{104,102}, P. Martinengo³⁴, J.L. Martinez¹²⁵, M.I. Martínez⁴⁴, G. Martínez García¹¹³, M. Martinez Pedreira³⁴, S. Masciocchi¹⁰⁴, M. Masera²⁶, A. Masoni⁵⁴, L. Massacrier⁶¹, E. Masson¹¹³, A. Mastroserio^{52,136}, A.M. Mathis^{116,103}, P.F.T. Matuoka¹²⁰, A. Matyjka^{117,128}, C. Mayer¹¹⁷, M. Mazzilli³³, M.A. Mazzoni⁵⁷, F. Meddi²³, Y. Melikyan⁹¹, A. Menchaca-Rocha⁷², E. Meninno³⁰, M. Meres¹⁴, S. Mhlanga¹²⁴, Y. Miake¹³¹, L. Micheletti²⁶, M.M. Mieskolainen⁴³, D.L. Mihaylov¹⁰³, K. Mikhaylov^{64,75}, A. Mischke⁶³, A.N. Mishra⁷⁰, D. Miśkowiec¹⁰⁴, J. Mitra¹³⁹, C.M. Mitu⁶⁸, N. Mohammadi³⁴, A.P. Mohanty⁶³, B. Mohanty⁸⁵, M. Mohisin Khan^{17,iv}, D.A. Moreira De Godoy¹⁴², L.A.P. Moreno⁴⁴, S. Moretto²⁹, A. Morreale¹¹³, A. Morsch³⁴, T. Mrnjavac³⁴, V. Muccifora⁵¹, E. Mudnic³⁵, D. Mühlheim¹⁴², S. Muhuri¹³⁹, M. Mukherjee³, J.D. Mulligan¹⁴⁴, M.G. Munhoz¹²⁰, K. Mürning⁴², M.I.A. Munoz⁷⁹, R.H. Munzer⁶⁹, H. Murakami¹³⁰, S. Murray⁷³, L. Musa³⁴, J. Musinsky⁶⁵, C.J. Myers¹²⁵, J.W. Myrcha¹⁴⁰, B. Naik⁴⁸, R. Nair⁸⁴, B.K. Nandi⁴⁸, R. Nania^{10,53}, E. Nappi⁵², A. Narayan⁴⁸, M.U. Naru¹⁵, A.F. Nassirpour⁸⁰, H. Natal da Luz¹²⁰, C. Natrass¹²⁸, S.R. Navarro⁴⁴, K. Nayak⁸⁵, R. Nayak⁴⁸, T.K. Nayak¹³⁹, S. Nazarenko¹⁰⁶, R.A. Negrao De Oliveira^{34,69}, L. Nellen⁷⁰, S.V. Nesbo³⁶, G. Neskovic³⁹, F. Ng¹²⁵, M. Nicassio¹⁰⁴, J. Niedziela^{140,34}, B.S. Nielsen⁸⁸, S. Nikolaev⁸⁷, S. Nikulin⁸⁷, V. Nikulin⁹⁶, F. Noferini^{10,53}, P. Nomokonov⁷⁵, G. Nooren⁶³, J.C.C. Noris⁴⁴, J. Norman⁷⁸, A. Nyanin⁸⁷, J. Nystrand²², M. Ogino⁸¹, H. Oh¹⁴⁵, A. Ohlson¹⁰², J. Oleniacz¹⁴⁰, A.C. Oliveira Da Silva¹²⁰, M.H. Oliver¹⁴⁴, J. Onderwaater¹⁰⁴, C. Oppedisano⁵⁸, R. Orava⁴³, M. Oravec¹¹⁵, A. Ortiz Velasquez⁷⁰, A. Oskarsson⁸⁰, J. Otwinowski¹¹⁷, K. Oyama⁸¹, Y. Pachmayer¹⁰², V. Pacik⁸⁸, D. Pagano¹³⁸, G. Paić⁷⁰, P. Palni⁶, J. Pan¹⁴¹, A.K. Pandey⁴⁸, S. Panebianco¹³⁵, V. Papikyan¹, P. Pareek⁴⁹, J. Park⁶⁰, J.E. Parkkila¹²⁶, S. Parmar⁹⁸, A. Passfeld¹⁴², S.P. Pathak¹²⁵, R.N. Patra¹³⁹, B. Paul⁵⁸, H. Pei⁶, T. Peitzmann⁶³, X. Peng⁶, L.G. Pereira⁷¹, H. Pereira Da Costa¹³⁵, D. Peresunko⁸⁷, E. Perez Lezama⁶⁹, V. Peskov⁶⁹, Y. Pestov⁴, V. Petráček³⁷, M. Petrovici⁴⁷, C. Petta²⁸, R.P. Pezzi⁷¹, S. Piano⁵⁹, M. Pikna¹⁴, P. Pillot¹¹³, L.O.D.L. Pimentel⁸⁸, O. Pinazza^{53,34}, L. Pinsky¹²⁵, S. Pisano⁵¹, D.B. Piyarathna¹²⁵, M. Płoskoń⁷⁹, M. Planinic⁹⁷, F. Pliquett⁶⁹, J. Pluta¹⁴⁰, S. Pochybova¹⁴³, P.L.M. Podesta-Lerma¹¹⁹, M.G. Poghosyan⁹⁴, B. Polichtchouk⁹⁰, N. Poljak⁹⁷, W. Poonsawat¹¹⁴, A. Pop⁴⁷, H. Poppenborg¹⁴², S. Porteboeuf-Houssais¹³², V. Pozdniakov⁷⁵, S.K. Prasad³, R. Preghenella⁵³, F. Prino⁵⁸, C.A. Pruneau¹⁴¹, I. Pshenichnov⁶², M. Puccio²⁶, V. Punin¹⁰⁶, K. Puranapanda¹³⁹, J. Putschke¹⁴¹, S. Raha³, S. Rajput⁹⁹, J. Rak¹²⁶, A. Rakotozafindrabe¹³⁵, L. Ramello³², F. Rami¹³⁴, R. Raniwala¹⁰⁰, S. Raniwala¹⁰⁰, S.S. Räsänen⁴³, B.T. Rascanu⁶⁹, R. Rath⁴⁹, V. Ratza⁴², I. Ravasenga³¹, K.F. Read^{128,94}, K. Redlich^{84,v}, A. Rehman²², P. Reichelt⁶⁹, F. Reidt³⁴, X. Ren⁶, R. Renfordt⁶⁹, A. Reshetin⁶², J.-P. Revol¹⁰, K. Reygers¹⁰², V. Riabov⁹⁶, T. Richert^{63,88,80}, M. Richter²¹,

P. Riedler³⁴, W. Riegler³⁴, F. Riggi²⁸, C. Ristea⁶⁸, S.P. Rode⁴⁹, M. Rodríguez Cahuantzi⁴⁴, K. Røed²¹, R. Rogalev⁹⁰, E. Rogochaya⁷⁵, D. Rohr³⁴, D. Röhrich²², P.S. Rokita¹⁴⁰, F. Ronchetti⁵¹, E.D. Rosas⁷⁰, K. Roslon¹⁴⁰, P. Rosnet¹³², A. Rossi^{56,29}, A. Rotondi¹³⁷, F. Roukoutakis⁸³, C. Roy¹³⁴, P. Roy¹⁰⁷, O.V. Rueda⁷⁰, R. Rui²⁵, B. Rumyantsev⁷⁵, A. Rustamov⁸⁶, E. Ryabinkin⁸⁷, Y. Ryabov⁹⁶, A. Rybicki¹¹⁷, S. Saarinen⁴³, S. Sadhu¹³⁹, S. Sadovsky⁹⁰, K. Šafařík³⁴, S.K. Saha¹³⁹, B. Sahoo⁴⁸, P. Sahoo⁴⁹, R. Sahoo⁴⁹, S. Sahoo⁶⁶, P.K. Sahu⁶⁶, J. Saini¹³⁹, S. Sakai¹³¹, M.A. Saleh¹⁴¹, S. Sambyal⁹⁹, V. Samsonov^{91,96}, A. Sandoval⁷², A. Sarkar⁷³, D. Sarkar¹³⁹, N. Sarkar¹³⁹, P. Sarma⁴¹, M.H.P. Sas⁶³, E. Scapparone⁵³, F. Scarlassara²⁹, B. Schaefer⁹⁴, H.S. Scheid⁶⁹, C. Schiaua⁴⁷, R. Schicker¹⁰², C. Schmidt¹⁰⁴, H.R. Schmidt¹⁰¹, M.O. Schmidt¹⁰², M. Schmidt¹⁰¹, N.V. Schmidt^{69,94}, J. Schukraft³⁴, Y. Schutz^{34,134}, K. Schwarz¹⁰⁴, K. Schweda¹⁰⁴, G. Scioli²⁷, E. Scomparin⁵⁸, M. Šefčík³⁸, J.E. Seger¹⁶, Y. Sekiguchi¹³⁰, D. Sekihata⁴⁵, I. Selyuzhenkov^{91,104}, S. Senyukov¹³⁴, E. Serradilla⁷², P. Sett⁴⁸, A. Sevcenco⁶⁸, A. Shabanov⁶², A. Shabetai¹¹³, R. Shahoyan³⁴, W. Shaikh¹⁰⁷, A. Shangaraev⁹⁰, A. Sharma⁹⁸, A. Sharma⁹⁹, M. Sharma⁹⁹, N. Sharma⁹⁸, A.I. Sheikh¹³⁹, K. Shigaki⁴⁵, M. Shimomura⁸², S. Shirinkin⁶⁴, Q. Shou^{6,110}, Y. Sibiriyak⁸⁷, S. Siddhanta⁵⁴, K.M. Sielewicz³⁴, T. Siemiarczuk⁸⁴, D. Silvermyr⁸⁰, G. Simatovic⁸⁹, G. Simonetti^{34,103}, R. Singaraju¹³⁹, R. Singh⁸⁵, R. Singh⁹⁹, V. Singhal¹³⁹, T. Sinha¹⁰⁷, B. Sitar¹⁴, M. Sitta³², T.B. Skaali²¹, M. Slupecki¹²⁶, N. Smirnov¹⁴⁴, R.J.M. Snellings⁶³, T.W. Snellman¹²⁶, J. Sochan¹¹⁵, C. Soncco¹⁰⁹, J. Song¹⁸, A. Songmoolnak¹¹⁴, F. Soramel²⁹, S. Sorensen¹²⁸, F. Sozzi¹⁰⁴, I. Sputowska¹¹⁷, J. Stachel¹⁰², I. Stan⁶⁸, P. Stankus⁹⁴, E. Stenlund⁸⁰, D. Stocco¹¹³, M.M. Storetvedt³⁶, P. Strmen¹⁴, A.A.P. Suaide¹²⁰, T. Sugitate⁴⁵, C. Suire⁶¹, M. Suleymanov¹⁵, M. Suljic³⁴, R. Sultanov⁶⁴, M. Šumbera⁹³, S. Sumowidagdo⁵⁰, K. Suzuki¹¹², S. Swain⁶⁶, A. Szabo¹⁴, I. Szarka¹⁴, U. Tabassam¹⁵, J. Takahashi¹²¹, G.J. Tambave²², N. Tanaka¹³¹, M. Tarhini¹¹³, M.G. Tarzila⁴⁷, A. Tauro³⁴, G. Tejada Muñoz⁴⁴, A. Telesca³⁴, C. Terrevoli²⁹, B. Teyssier¹³³, D. Thakur⁴⁹, S. Thakur¹³⁹, D. Thomas¹¹⁸, F. Thoresen⁸⁸, R. Tieulent¹³³, A. Tikhonov⁶², A.R. Timmins¹²⁵, A. Toia⁶⁹, N. Topilskaya⁶², M. Toppi⁵¹, S.R. Torres¹¹⁹, S. Tripathy⁴⁹, S. Trogolo²⁶, G. Trombetta³³, L. Tropp³⁸, V. Trubnikov², W.H. Trzaska¹²⁶, T.P. Trzcinski¹⁴⁰, B.A. Trzeciak⁶³, T. Tsuji¹³⁰, A. Tumkin¹⁰⁶, R. Turrisi⁵⁶, T.S. Tveter²¹, K. Ullaland²², E.N. Umaka¹²⁵, A. Uras¹³³, G.L. Usai²⁴, A. Utrobicic⁹⁷, M. Vala¹¹⁵, L. Valencia Palomo⁴⁴, N. Valle¹³⁷, N. van der Kolk⁶³, L.V.R. van Doremalen⁶³, J.W. Van Hoorne³⁴, M. van Leeuwen⁶³, P. Vande Vyvre³⁴, D. Varga¹⁴³, A. Vargas⁴⁴, M. Vargyas¹²⁶, R. Varma⁴⁸, M. Vasileiou⁸³, A. Vasiliev⁸⁷, O. Vázquez Doce^{103,116}, V. Vechernin¹¹¹, A.M. Veen⁶³, E. Vercellin²⁶, S. Vergara Limón⁴⁴, L. Vermunt⁶³, R. Vernet⁷, R. Vértesi¹⁴³, L. Vickovic³⁵, J. Viinikainen¹²⁶, Z. Vilakazi¹²⁹, O. Villalobos Baillie¹⁰⁸, A. Villatoro Tello⁴⁴, A. Vinogradov⁸⁷, T. Virgili³⁰, V. Vislavicius^{80,88}, A. Vodopyanov⁷⁵, M.A. Völkl¹⁰¹, K. Voloshin⁶⁴, S.A. Voloshin¹⁴¹, G. Volpe³³, B. von Haller³⁴, I. Vorobyev^{116,103}, D. Voscek¹¹⁵, D. Vranic^{34,104}, J. Vrláková³⁸, B. Wagner²², M. Wang⁶, Y. Watanabe¹³¹, M. Weber¹¹², S.G. Weber¹⁰⁴, A. Wegrzynek³⁴, D.F. Weiser¹⁰², S.C. Wenzel³⁴, J.P. Wessels¹⁴², U. Westerhoff¹⁴², A.M. Whitehead¹²⁴, J. Wiechula⁶⁹, J. Wikne²¹, G. Wilk⁸⁴, J. Wilkinson⁵³, G.A. Willems^{142,34}, M.C.S. Williams⁵³, E. Willsher¹⁰⁸, B. Windelband¹⁰², W.E. Witt¹²⁸, R. Xu⁶, S. Yalcin⁷⁷, K. Yamakawa⁴⁵, S. Yano^{135,45}, Z. Yin⁶, H. Yokoyama^{131,78}, I.-K. Yoo¹⁸, J.H. Yoon⁶⁰, V. Yurchenko², V. Zaccolo⁵⁸, A. Zaman¹⁵, C. Zampolli³⁴, H.J.C. Zanoli¹²⁰, N. Zardoshti¹⁰⁸, A. Zarochentsev¹¹¹, P. Závada⁶⁷, N. Zaviyalov¹⁰⁶, H. Zbroszczyk¹⁴⁰, M. Zhalov⁹⁶, X. Zhang⁶, Y. Zhang⁶, Z. Zhang^{132,6}, C. Zhao²¹, V. Zherebchevskii¹¹¹, N. Zhigareva⁶⁴, D. Zhou⁶, Y. Zhou⁸⁸, Z. Zhou²², H. Zhu⁶, J. Zhu⁶, Y. Zhu⁶, A. Zichichi^{10,27}, M.B. Zimmermann³⁴, G. Zinovjev², J. Zmeskal¹¹²,

Affiliation notes

ⁱ Deceased

ⁱⁱ Dipartimento DET del Politecnico di Torino, Turin, Italy

ⁱⁱⁱ M.V. Lomonosov Moscow State University, D.V. Skobeltsyn Institute of Nuclear Physics, Moscow, Russia

^{iv} Department of Applied Physics, Aligarh Muslim University, Aligarh, India

^v Institute of Theoretical Physics, University of Wrocław, Poland

Collaboration Institutes

¹ A.I. Alikhanyan National Science Laboratory (Yerevan Physics Institute) Foundation, Yerevan, Armenia

² Bogolyubov Institute for Theoretical Physics, National Academy of Sciences of Ukraine, Kiev, Ukraine

³ Bose Institute, Department of Physics and Centre for Astroparticle Physics and Space Science (CAPSS), Kolkata, India

⁴ Budker Institute for Nuclear Physics, Novosibirsk, Russia

⁵ California Polytechnic State University, San Luis Obispo, California, United States

- 6 Central China Normal University, Wuhan, China
- 7 Centre de Calcul de l'IN2P3, Villeurbanne, Lyon, France
- 8 Centro de Aplicaciones Tecnológicas y Desarrollo Nuclear (CEADEN), Havana, Cuba
- 9 Centro de Investigación y de Estudios Avanzados (CINVESTAV), Mexico City and Mérida, Mexico
- 10 Centro Fermi - Museo Storico della Fisica e Centro Studi e Ricerche "Enrico Fermi", Rome, Italy
- 11 Chicago State University, Chicago, Illinois, United States
- 12 China Institute of Atomic Energy, Beijing, China
- 13 Chonbuk National University, Jeonju, Republic of Korea
- 14 Comenius University Bratislava, Faculty of Mathematics, Physics and Informatics, Bratislava, Slovakia
- 15 COMSATS Institute of Information Technology (CIIT), Islamabad, Pakistan
- 16 Creighton University, Omaha, Nebraska, United States
- 17 Department of Physics, Aligarh Muslim University, Aligarh, India
- 18 Department of Physics, Pusan National University, Pusan, Republic of Korea
- 19 Department of Physics, Sejong University, Seoul, Republic of Korea
- 20 Department of Physics, University of California, Berkeley, California, United States
- 21 Department of Physics, University of Oslo, Oslo, Norway
- 22 Department of Physics and Technology, University of Bergen, Bergen, Norway
- 23 Dipartimento di Fisica dell'Università 'La Sapienza' and Sezione INFN, Rome, Italy
- 24 Dipartimento di Fisica dell'Università and Sezione INFN, Cagliari, Italy
- 25 Dipartimento di Fisica dell'Università and Sezione INFN, Trieste, Italy
- 26 Dipartimento di Fisica dell'Università and Sezione INFN, Turin, Italy
- 27 Dipartimento di Fisica e Astronomia dell'Università and Sezione INFN, Bologna, Italy
- 28 Dipartimento di Fisica e Astronomia dell'Università and Sezione INFN, Catania, Italy
- 29 Dipartimento di Fisica e Astronomia dell'Università and Sezione INFN, Padova, Italy
- 30 Dipartimento di Fisica 'E.R. Caianiello' dell'Università and Gruppo Collegato INFN, Salerno, Italy
- 31 Dipartimento DISAT del Politecnico and Sezione INFN, Turin, Italy
- 32 Dipartimento di Scienze e Innovazione Tecnologica dell'Università del Piemonte Orientale and INFN Sezione di Torino, Alessandria, Italy
- 33 Dipartimento Interateneo di Fisica 'M. Merlin' and Sezione INFN, Bari, Italy
- 34 European Organization for Nuclear Research (CERN), Geneva, Switzerland
- 35 Faculty of Electrical Engineering, Mechanical Engineering and Naval Architecture, University of Split, Split, Croatia
- 36 Faculty of Engineering and Science, Western Norway University of Applied Sciences, Bergen, Norway
- 37 Faculty of Nuclear Sciences and Physical Engineering, Czech Technical University in Prague, Prague, Czech Republic
- 38 Faculty of Science, P.J. Šafárik University, Košice, Slovakia
- 39 Frankfurt Institute for Advanced Studies, Johann Wolfgang Goethe-Universität Frankfurt, Frankfurt, Germany
- 40 Gangneung-Wonju National University, Gangneung, Republic of Korea
- 41 Gauhati University, Department of Physics, Guwahati, India
- 42 Helmholtz-Institut für Strahlen- und Kernphysik, Rheinische Friedrich-Wilhelms-Universität Bonn, Bonn, Germany
- 43 Helsinki Institute of Physics (HIP), Helsinki, Finland
- 44 High Energy Physics Group, Universidad Autónoma de Puebla, Puebla, Mexico
- 45 Hiroshima University, Hiroshima, Japan
- 46 Hochschule Worms, Zentrum für Technologietransfer und Telekommunikation (ZTT), Worms, Germany
- 47 Horia Hulubei National Institute of Physics and Nuclear Engineering, Bucharest, Romania
- 48 Indian Institute of Technology Bombay (IIT), Mumbai, India
- 49 Indian Institute of Technology Indore, Indore, India
- 50 Indonesian Institute of Sciences, Jakarta, Indonesia
- 51 INFN, Laboratori Nazionali di Frascati, Frascati, Italy
- 52 INFN, Sezione di Bari, Bari, Italy
- 53 INFN, Sezione di Bologna, Bologna, Italy
- 54 INFN, Sezione di Cagliari, Cagliari, Italy
- 55 INFN, Sezione di Catania, Catania, Italy
- 56 INFN, Sezione di Padova, Padova, Italy

- 57 INFN, Sezione di Roma, Rome, Italy
- 58 INFN, Sezione di Torino, Turin, Italy
- 59 INFN, Sezione di Trieste, Trieste, Italy
- 60 Inha University, Incheon, Republic of Korea
- 61 Institut de Physique Nucléaire d'Orsay (IPNO), Institut National de Physique Nucléaire et de Physique des Particules (IN2P3/CNRS), Université de Paris-Sud, Université Paris-Saclay, Orsay, France
- 62 Institute for Nuclear Research, Academy of Sciences, Moscow, Russia
- 63 Institute for Subatomic Physics, Utrecht University/Nikhef, Utrecht, Netherlands
- 64 Institute for Theoretical and Experimental Physics, Moscow, Russia
- 65 Institute of Experimental Physics, Slovak Academy of Sciences, Košice, Slovakia
- 66 Institute of Physics, Homi Bhabha National Institute, Bhubaneswar, India
- 67 Institute of Physics of the Czech Academy of Sciences, Prague, Czech Republic
- 68 Institute of Space Science (ISS), Bucharest, Romania
- 69 Institut für Kernphysik, Johann Wolfgang Goethe-Universität Frankfurt, Frankfurt, Germany
- 70 Instituto de Ciencias Nucleares, Universidad Nacional Autónoma de México, Mexico City, Mexico
- 71 Instituto de Física, Universidade Federal do Rio Grande do Sul (UFRGS), Porto Alegre, Brazil
- 72 Instituto de Física, Universidad Nacional Autónoma de México, Mexico City, Mexico
- 73 iThemba LABS, National Research Foundation, Somerset West, South Africa
- 74 Johann-Wolfgang-Goethe Universität Frankfurt Institut für Informatik, Fachbereich Informatik und Mathematik, Frankfurt, Germany
- 75 Joint Institute for Nuclear Research (JINR), Dubna, Russia
- 76 Korea Institute of Science and Technology Information, Daejeon, Republic of Korea
- 77 KTO Karatay University, Konya, Turkey
- 78 Laboratoire de Physique Subatomique et de Cosmologie, Université Grenoble-Alpes, CNRS-IN2P3, Grenoble, France
- 79 Lawrence Berkeley National Laboratory, Berkeley, California, United States
- 80 Lund University Department of Physics, Division of Particle Physics, Lund, Sweden
- 81 Nagasaki Institute of Applied Science, Nagasaki, Japan
- 82 Nara Women's University (NWU), Nara, Japan
- 83 National and Kapodistrian University of Athens, School of Science, Department of Physics, Athens, Greece
- 84 National Centre for Nuclear Research, Warsaw, Poland
- 85 National Institute of Science Education and Research, Homi Bhabha National Institute, Jatni, India
- 86 National Nuclear Research Center, Baku, Azerbaijan
- 87 National Research Centre Kurchatov Institute, Moscow, Russia
- 88 Niels Bohr Institute, University of Copenhagen, Copenhagen, Denmark
- 89 Nikhef, National institute for subatomic physics, Amsterdam, Netherlands
- 90 NRC Kurchatov Institute IHEP, Protvino, Russia
- 91 NRNU Moscow Engineering Physics Institute, Moscow, Russia
- 92 Nuclear Physics Group, STFC Daresbury Laboratory, Daresbury, United Kingdom
- 93 Nuclear Physics Institute of the Czech Academy of Sciences, Řež u Prahy, Czech Republic
- 94 Oak Ridge National Laboratory, Oak Ridge, Tennessee, United States
- 95 Ohio State University, Columbus, Ohio, United States
- 96 Petersburg Nuclear Physics Institute, Gatchina, Russia
- 97 Physics department, Faculty of science, University of Zagreb, Zagreb, Croatia
- 98 Physics Department, Panjab University, Chandigarh, India
- 99 Physics Department, University of Jammu, Jammu, India
- 100 Physics Department, University of Rajasthan, Jaipur, India
- 101 Physikalisches Institut, Eberhard-Karls-Universität Tübingen, Tübingen, Germany
- 102 Physikalisches Institut, Ruprecht-Karls-Universität Heidelberg, Heidelberg, Germany
- 103 Physik Department, Technische Universität München, Munich, Germany
- 104 Research Division and ExtreMe Matter Institute EMMI, GSI Helmholtzzentrum für Schwerionenforschung GmbH, Darmstadt, Germany
- 105 Rudjer Bošković Institute, Zagreb, Croatia
- 106 Russian Federal Nuclear Center (VNIIEF), Sarov, Russia
- 107 Saha Institute of Nuclear Physics, Homi Bhabha National Institute, Kolkata, India

- 108 School of Physics and Astronomy, University of Birmingham, Birmingham, United Kingdom
- 109 Sección Física, Departamento de Ciencias, Pontificia Universidad Católica del Perú, Lima, Peru
- 110 Shanghai Institute of Applied Physics, Shanghai, China
- 111 St. Petersburg State University, St. Petersburg, Russia
- 112 Stefan Meyer Institut für Subatomare Physik (SMI), Vienna, Austria
- 113 SUBATECH, IMT Atlantique, Université de Nantes, CNRS-IN2P3, Nantes, France
- 114 Suranaree University of Technology, Nakhon Ratchasima, Thailand
- 115 Technical University of Košice, Košice, Slovakia
- 116 Technische Universität München, Excellence Cluster 'Universe', Munich, Germany
- 117 The Henryk Niewodniczanski Institute of Nuclear Physics, Polish Academy of Sciences, Cracow, Poland
- 118 The University of Texas at Austin, Austin, Texas, United States
- 119 Universidad Autónoma de Sinaloa, Culiacán, Mexico
- 120 Universidade de São Paulo (USP), São Paulo, Brazil
- 121 Universidade Estadual de Campinas (UNICAMP), Campinas, Brazil
- 122 Universidade Federal do ABC, Santo Andre, Brazil
- 123 University College of Southeast Norway, Tonsberg, Norway
- 124 University of Cape Town, Cape Town, South Africa
- 125 University of Houston, Houston, Texas, United States
- 126 University of Jyväskylä, Jyväskylä, Finland
- 127 University of Liverpool, Liverpool, United Kingdom
- 128 University of Tennessee, Knoxville, Tennessee, United States
- 129 University of the Witwatersrand, Johannesburg, South Africa
- 130 University of Tokyo, Tokyo, Japan
- 131 University of Tsukuba, Tsukuba, Japan
- 132 Université Clermont Auvergne, CNRS/IN2P3, LPC, Clermont-Ferrand, France
- 133 Université de Lyon, Université Lyon 1, CNRS/IN2P3, IPN-Lyon, Villeurbanne, Lyon, France
- 134 Université de Strasbourg, CNRS, IPHC UMR 7178, F-67000 Strasbourg, France, Strasbourg, France
- 135 Université Paris-Saclay Centre d'Études de Saclay (CEA), IRFU, Department de Physique Nucléaire (DPhN), Saclay, France
- 136 Università degli Studi di Foggia, Foggia, Italy
- 137 Università degli Studi di Pavia, Pavia, Italy
- 138 Università di Brescia, Brescia, Italy
- 139 Variable Energy Cyclotron Centre, Homi Bhabha National Institute, Kolkata, India
- 140 Warsaw University of Technology, Warsaw, Poland
- 141 Wayne State University, Detroit, Michigan, United States
- 142 Westfälische Wilhelms-Universität Münster, Institut für Kernphysik, Münster, Germany
- 143 Wigner Research Centre for Physics, Hungarian Academy of Sciences, Budapest, Hungary
- 144 Yale University, New Haven, Connecticut, United States
- 145 Yonsei University, Seoul, Republic of Korea